ARTICLE

https://doi.org/10.1590/2317-4889202120210046

BJGEO
Brazilian Journal of Geology

New high-precision $^{40}Ar/^{39}Ar$ ages for the Serra do Mar alkaline magmatism in the São Sebastião Island, SE Brazil, and implications

Maria Isabel Giraldo-Arroyave[1]*, Silvio Roberto Farias Vlach[1], Paulo Marcos Vasconcelos[2]

Abstract

We present new high-resolution $^{40}Ar/^{39}Ar$ ages for alkaline layered gabbros and cross-cutting mafic-ultramafic and felsic dykes from the São Sebastião Island, in the northern sector of the Serra do Mar Alkaline Province, São Paulo, Brazil. Duplicate analysis of single kaersutite crystals yielded plateau ages of 88 ± 1 and 87.9 ± 0.8 Ma for a gabbro and 87 ± 1 and 86.0 ± 0.8 Ma for a picrite dyke. Two biotite aliquots from a trachyte yielded ages of 86.0 ± 0.5 and 86.2 ± 0.5 Ma, while an alkali feldspar concentrate yielded ages of 86.0 ± 0.5 Ma. The similar ages obtained for minerals with contrasting closure temperatures suggest that the results are crystallization ages and that the rocks were emplaced at shallow crustal levels. Our results, along with available high-resolution data, point to a relatively narrow time span (*ca.* 88-85 ± 0.6 Ma) for the entire alkaline magmatism on the island. Other alkaline occurrences both nearby and in the continent's interior reveal similar ages, reinforcing the hypothesis that mantle decompression and upwelling of heterogeneous mantle sources led to crustal extension and fast ascension of a variety of alkaline magma types in this segment of South America.

KEYWORDS: $^{40}Ar/^{39}Ar$ geochronology; mafic-ultramafic and felsic alkaline rocks; São Sebastião Island; Serra do Mar Province; SE Brazil.

INTRODUCTION

Continental flood basalts and associated dyke swarms, mafic-ultramafic layered intrusions and bimodal magmatic suites are key markers of extensional tectonics and continental rifting preceding ocean basin formation (White and McKenzie 1989, Amelin *et al.* 1995, Bernstein *et al.* 1996, Ernst *et al.* 2005). They are typical features related to Meso-Cenozoic Gondwana breakup in the southeastern South American Platform. Three main periods of extensive magmatic activity have been identified based on geological and geochronological data (e.g., Amaral *et al.* 1967, Almeida 1983, Ulbrich *et al.* 1991, Riccomini *et al.* 2005). The first event, in the Early Cretaceous (*ca.* 134-130 Ma), corresponds to the earliest rifting stage before Gondwana break-up, resulting in the extensive tholeiitic and minor silicic magmatism of the Paraná-Etendeka Large Igneous Province, as well as some roughly contemporaneous alkaline-carbonatite complexes (Ulbrich *et al.* 1991, Renne *et al.* 1992, Renne *et al.* 1996, Thiede and Vasconcelos 2010, Gomes and Vasconcelos 2021). The second event, in the Aptian-Conician (*ca.* 110-80 Ma), is characterized by the emplacement of a variety of alkaline-carbonatite intrusions (Poços de Caldas, Itatiaia, Passa Quatro and Ponte Nova Massifs), and it records progressive crustal extension and ocean opening along ancient Neoproterozoic shear zones (e.g., Amaral *et al.* 1967, Ulbrich and Gomes 1981, Almeida 1983, Velázquez 1996, Ulbrich *et al.* 2005, Azzone *et al.* 2009). The youngest event, occurring during the Paleocene-Eocene (*ca.* 65-45 Ma), is registered in the sodic alkaline volcanic rocks in the western segment of the Asunción Rift (Almeida 1983, Comin-Chiaramonti *et al.* 1997) and in the Brazilian Continental Southeastern Rift (Resende, Cabo Frio, Búzios), resulting mainly from lithospheric decompression along active deep faults (e.g., Riccomini *et al.* 2001).

In the state of São Paulo (Fig. 1A), crustal extension and Late Cretaceous alkaline magmatism are registered along the coast and in some nearby islands (São Sebastião, Monte do Trigo, Búzios and Vitória). These occurrences, along with the mafic-ultramafic Ponte Nova Massif in Minas Gerais and several intrusive units in Rio de Janeiro, were originally considered part of the Serra do Mar Alkaline Province (Almeida 1983, Almeida and Carneiro 1998), and later grouped with the northern sector of this province (Riccomini *et al.* 2005). This alkaline magmatism is bimodal, hosting a variety of SiO_2-undersaturated and -oversaturated syenite varieties and minor gabbroic rocks, accompanied by a variety of SiO_2-undersaturated (from ultrabasic lamprophyres, pyroxenites to phonolites) to marginally -saturated (alkali basalts, microgabbros to trachytes) dykes (e.g., Ulbrich and Gomes 1981, Bellieni *et al.* 1990, Brotzu *et al.* 2005, Enrich *et al.* 2005, Azzone *et al.* 2009).

Since the pioneering work of Amaral *et al.* (1967), geochronological information on the alkaline magmatism in southeastern Brazil has improved significantly (e.g., Sonoki and Garda

[1]Institute of Geosciences, Universidade de São Paulo – São Paulo (SP), Brazil. E-mails: mariageologa@gmail.com, srfvlach@usp.br

[2]School of Earth and Environmental Sciences, University of Queensland – Brisbane, Australia. E-mail: p.vasconcelos@uq.edu.au

*Corresponding author.

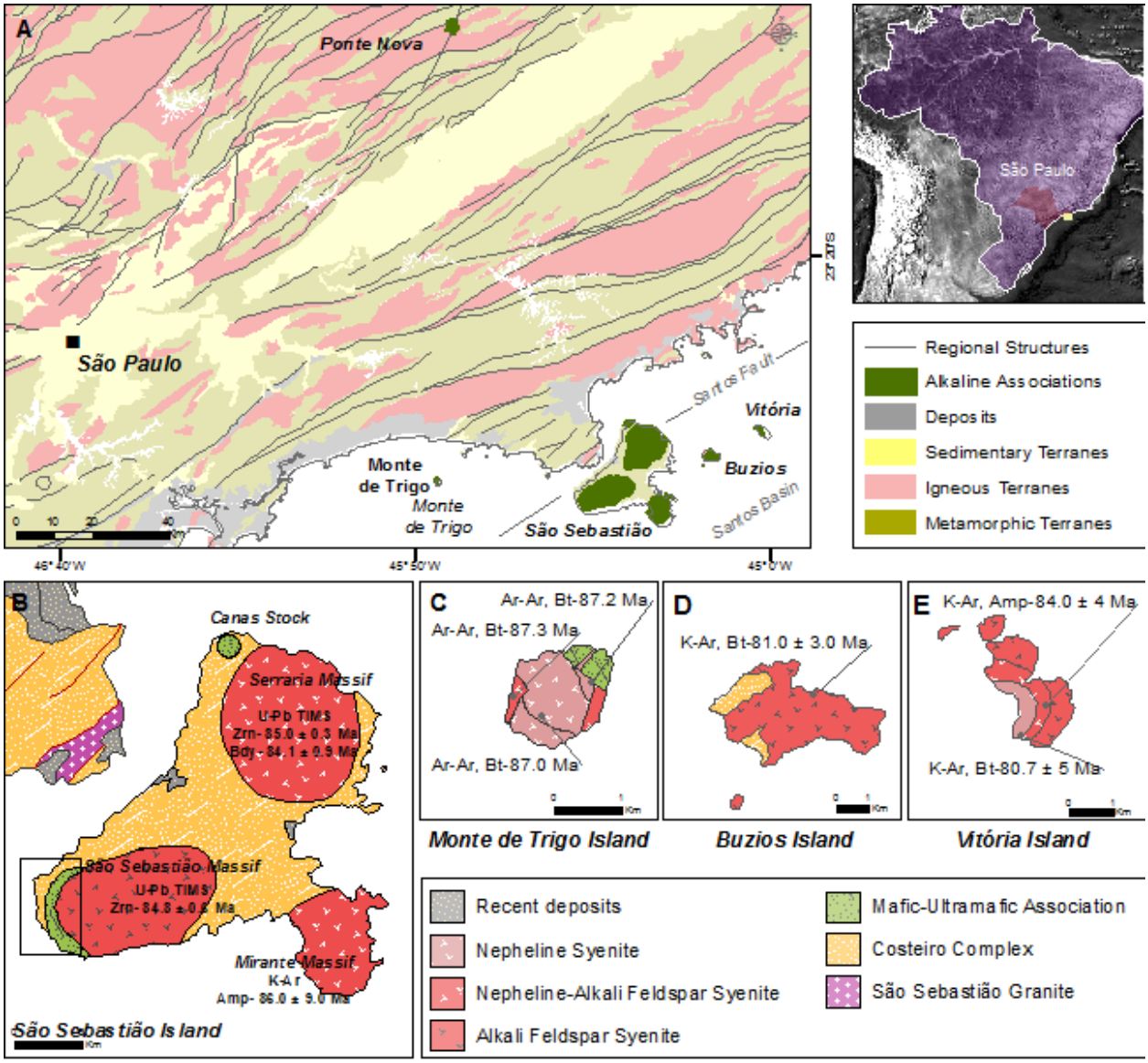

Figure 1. Simplified geological map of the Mantiqueira Province, northern sector of the São Paulo state, showing the alkaline association of the Serra do Mar Province (Geological Survey of Brazil-CPRM); (B, C and E) the simplified geology of the São Sebastião Island (Freitas 1947, Hennies and Hasui 1977, Bellieni *et al.* 1990); Monte de Trigo Island (Enrich *et al.* 2009); (D) Búzios Island (Alves and Gomes 2001) and Vitoria Island (Motoki 1986), respectively. All ages shown are previous data compiled from literature.

1988, Bellieni *et al.* 1990, Ulbrich *et al.* 1991, Montes-Lauar *et al.* 1995, Sato *et al.* 2008, Enrich *et al.* 2009, Gomes *et al.* 2017). The available data indicates that magmatic activity in the northern sector of the Serra do Mar Province spans from *ca.* 90 to 80 Ma. However, the paucity of high-resolution geochronology results prevents resolving the detailed stratigraphy of short-range magmatic events, making it difficult to examine and correlate the main emplacement mechanisms and petrological processes associated with magma generation, the evolution of plumbing systems in each occurrence, and their geodynamic environments.

To address some of these issues, we conducted new single crystal $^{40}Ar/^{39}Ar$ laser incremental-heating geochronology in amphibole, biotite and alkali feldspar from selected gabbro samples from a layered alkaline intrusion as well as cross-cutting mafic-ultramafic and felsic dykes in the southern area of the São Sebastião Island, northeastern São Paulo. We combine the geochronological results with petrographic, petrological and geochemical investigation in order to constrain the duration of silicic and basic-ultrabasic alkaline magma generation and emplacement into the upper crust. The results, along with other existing high-precision ages, give new insights into the sequence and time span of alkaline magmatism in the island, which may also extend to the Serra do Mar Province.

GEOLOGICAL BACKGROUND

Most alkaline occurrences related to the Meso-Cenozoic continental rifting in southeastern Brazil are distributed along the margins of the Paraná Sedimentary Basin, and were grouped into several provinces based on geological, geochronological, petrographic and geochemical data, as well as geodynamic settings (Ulbrich and Gomes 1981, Almeida 1983, Riccomini *et al.* 2005).

In the northern sector of the Serra do Mar Province, the rocks are predominantly felsic and made up mainly of SiO_2-oversaturated alkali feldspar syenites and quartz-alkali feldspar syenites (Bellieni *et al.* 1990, Alves 1997, Alves and Gomes 2001, Augusto 2003, Gomes *et al.* 2017), SiO_2-undersaturated nepheline syenites and nepheline alkali feldspar syenites (Motoki 1986, Enrich 2005, Enrich *et al.* 2009), and associated trachyte and phonolite dykes. Closely associated plutonic mafic-ultramafic alkaline rocks, represented by gabbros and minor clinopyroxenites, occur as layered intrusions in the São Sebastião and Monte do Trigo islands. Lamprophyres, micropyroxenites and associated dykes are distributed along the Atlantic margin and nearby islands (Coutinho and Melcher 1973, Sonoki and Garda 1988, Bellieni *et al.* 1990). Towards the continental interior, the Ponte Nova Massif represents the major exposure of mafic and ultramafic rocks of alkaline affinity (Azzone *et al.* 2009).

The São Sebastião Island (Fig. 1A) is a detached fragment of the Costeiro Complex, the easternmost domain of the Neoproterozoic Central Ribeira Belt (Almeida 1983, Heilbron and Machado 2003), separated from the continent by the NE-SW Santos Fault System during the Cretaceous continental rift (*e.g.*, Riccomini *et al.* 2005). It is the largest island in the area, covering ~ 340 km^2, and it comprises Neoproterozoic country rocks, Late Cretaceous alkaline intrusions and dykes of various compositions (Fig. 1B).

The Costeiro Complex is composed of Neoproterozoic medium- to high-grade metamorphic rocks, migmatites, intrusive granites and some charnokites.

Felsic alkaline plutonic rocks are dominant and make up three roughly subcircular intrusions: the larger Serraria (to the north), the São Sebastião (to the south) and the minor Mirante massifs (to the east). Serraria and São Sebastião comprise mostly SiO_2-oversaturated alkali feldspar syenites and quartz alkali feldspar syenites, while Mirante includes both SiO_2-oversaturated and -undersaturated rocks (Freitas 1947, Hennies and Hasui 1977, Bellieni *et al.* 1990, Augusto 2003, Sato 2006).

Layered mafic-ultramafic alkaline plutonic rocks are subordinated and crop out in the southern and northern areas in the island (Fig. 1B). They are made up of gabbroic rocks accompanied by minor pyroxenites, as well as scarce peridotites and anorthosites. Northwards, they appear in the Ponta das Canas, Pacuíba and neighboring coastal areas (Freitas 1947, Piccirillo *et al.* 1990, Lima 2001, Timich *et al.* 2019) and southwards they crop out at the Borrifos and Frade areas (Augusto 2003, Pabst 2014). Magmatic structures are similar to those typically observed in layered mafic-ultramafic complexes (*e.g.*, Alapieti *et al.* 1990, Eales and Cawthorn 1996, Emeleus *et al.* 1996, McCallum 1996, Wilson *et al.* 1996) and are best seen in the northern areas, where they were accentuated by surface sea-water weathering. In this area, however, the outcrops are mostly represented by loose boulders and the spatial distribution of the structures as well as the magmatic stratigraphy cannot be mapped. Fresh and more or less continuous *in situ* outcrops are known solely in the southern area investigated here.

Dykes trend mainly NE and have been subdivided into two main groups based on structural relationships with the syenitic rocks (Hennies and Hasui 1977, Bellieni *et al.* 1990): a Lower Cretaceous group, comprising dominantly basic dykes related to tholeiitic magmatism from the Paraná Magmatic Province that yield ages in the 134-130 Ma range (Turner *et al.* 1994, Renne *et al.* 1996, Deckart *et al.* 1998); and mafic-ultramafic and felsic dykes with alkaline affinity and emplaced at *ca.* 90-70 Ma (e.g., Sonoki and Garda 1988, Bellieni *et al.* 1990).

Previous geochronological data

There have been numerous attempts to constrain the temporal framework of alkaline magmatism in the São Sebastião and neighboring islands and continental areas (Figs. 1B–1E). However, most results are derived from mineral and/or whole-rock K/Ar (Amaral *et al.* 1967, Hennies and Hasui 1977, Motoki 1986, Sonoki and Garda 1988, Bellieni *et al.* 1990, Alves 1997, Azzone *et al.* 2009) and Rb/Sr methods (Motoki 1986, Montes-Lauar *et al.* 1995), with limited high-precision zircon U/Pb ages (Sato 2006, Sato *et al.* 2008) and $^{40}Ar/^{39}Ar$ (Enrich 2005, Enrich *et al.* 2009). The results reveal predominant Upper Cretaceous ages, between *ca.* 90 and 80 Ma; however, most K/Ar and Rb/Sr ages show significant scatter, even for similar rocks, and the relatively large uncertainties (up to 10 Ma) prevents discriminating the magmatic events and determining their duration.

Enrich *et al.* (2009) obtained high-precision $^{40}Ar/^{39}Ar$ ages for the alkaline rocks from the nearby Monte do Trigo Island. Biotite plateau ages, herein corrected for the new recommended ages for the Fish Canyon Sanidine Standard (*cf.* Kuiper *et al.* 2008), yielded values ranging from 87.8 to 86.6 (± 0.5 Ma) Ma for gabbroic rocks and nepheline syenites, respectively. A biotite lamprophyre yielded similar results, whereas a peralkaline phonolite dyke show a younger age of 84.9 (± 1.0 Ma) Ma. The ages of the plutonic rocks in this island are similar to the estimated weighted average K-Ar age for the emplacement of the mafic-ultramafic Ponte Nova Massif in the continental interior (87.6 ± 1.3 Ma, Azzone *et al.* 2009).

In the São Sebastião Island, previous K/Ar ages in biotite, amphibole, and alkali feldspars from the felsic intrusions show a relatively large span from 87 ± 5 to 81 ± 6 Ma, while biotite crystals from felsic dykes yield ages ranging from 83 ± 6 to 78 ± 8 Ma. Gabbroic rocks yield older results (99 ± 3 to 87 ± 5 Ma; *cf.* Amaral *et al.* 1967, Hennies and Hasui 1977, Sonoki and Garda 1988). A Rb/Sr isochron for the felsic intrusive rocks, combining mineral concentrates and whole-rock analyses, yielded a reference age of ~ 81 ± 3 Ma (Montes-Lauar *et al.* 1995). High-precision U/Pb (ID-TIMS) zircon results obtained for SiO_2-oversaturated alkali feldspar syenites yielded concordant U/Pb ages of 84.8 ± 0.7 Ma and 85.0 ± 0.3 Ma for the São Sebastião and Serraria massifs respectively, while baddeleyite yielded ages of 84.1 ± 1.0 Ma for the Serraria sample (Sato 2006, Sato *et al.* 2008). These results indicated the almost coeval character of the main SiO_2-oversaturated felsic plutonic rocks.

SAMPLING AND ANALYTICAL PROCEDURES

Based on the available geochronological data and our new geologic and petrographic data (Giraldo-Arroyave 2020), we selected three pristine samples (Fig. 2) with potential to yield

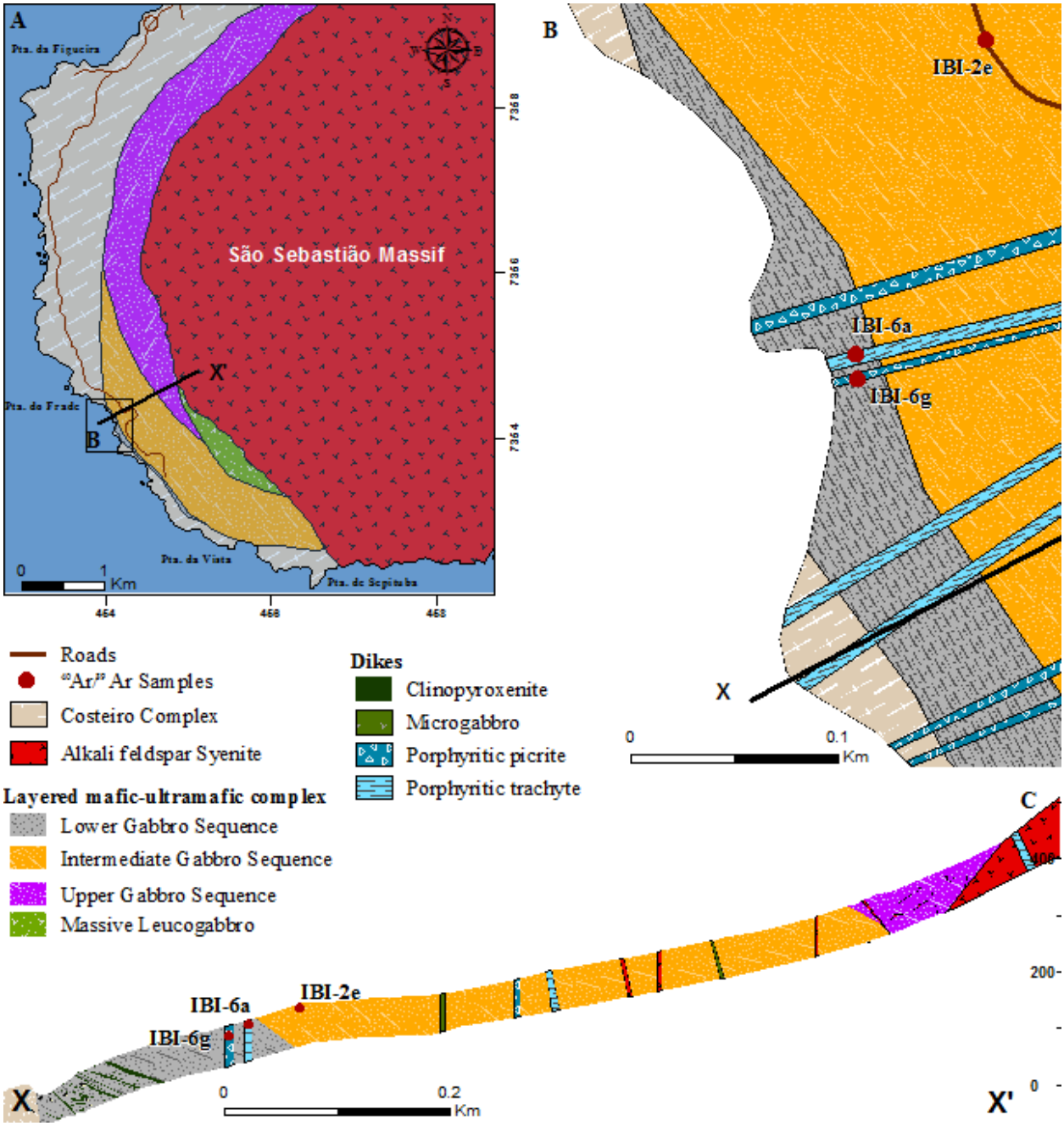

Figure 2. Detailed geologic map of the mafic-ultramafic layered intrusive south of the São Sebastião Island (Giraldo-Arroyave 2020). (A and B) Selected sample locations. (C) Schematic cross-section (X-X') through the layered sequence, crosscutting dikes and the São Sebastião Massif.

reliable crystallization ages for the alkaline magmatism in the São Sebastião Island: an olivine gabbro (sample IBI-2e) from the southern layered complex; and two cross-cutting dykes, a picrite (IBI-6g) and a trachyte (IBI-06a), representing the main ultramafic and felsic rocks, respectively. $^{40}Ar/^{39}Ar$ dating was carried on interstitial (IBI-2e) and groundmass (IBI-6g) kaersutitic amphibole and biotite and alkali feldspar phenocrysts (IBI-06a).

Sample preparation and analysis were performed at the GeoAnalitica core facility (Universidade de São Paulo, BR), whereas sample irradiation and isotopic Ar analysis were performed at the Cadmiun-lined-B-1 CLICIT facility (Oregon State University, USA) and UQ-AGES (University of Queensland Argon Geochronology in Earth Sciences Laboratory), Australia, respectively.

Polished thin sections were described in transmitted and reflected light in order to determine rock mineralogy, texture, and modal mineral contents, estimated via point counting. Mineral zoning patterns were examined in electron backscattered images (BEI) and their chemical compositions were determined via wavelength dispersive X-ray spectrometry (WDS), using the JEOL JXA-FE-8530 electron probe micro-analyzer (EPMA). WDS analysis was performed in carbon-coated samples under 15 kV accelerating voltage, 20 nA beam current and 5-10 µm beam diameter using conventional laboratory routines (*e.g.*,

Gualda and Vlach 2007) and natural and synthetic standards from the Smithsonian Institute. Matrix effects were corrected using the PRZ-Armstrong approach implemented in the JEOL software. Cation proportions and the partition between Fe^{2+} and Fe^{3+}, assuming the maximum Fe^{3+} criteria of Schumacher (Leake *et al.* 1997), were achived using the MinCal software (Gualda and Vlach 2005). Given the potential influence of subsolidus transformations of the alkali feldspars on $^{40}Ar/^{39}Ar$ dating, the structural state of the sampled alkali feldspar grains was examined by X-ray diffraction under Cu Kα radiation, using a Siemens XRD Diffractometer D5000.

The samples were crushed in a jaw-crusher and sieved, then split into different size fractions. Magnetic and non-magnetic fractions were obtained using a Frantz isodynamic separator under magnetic fields induced by 0.4 and 0.5 A electric currents, from which mineral fractions were hand-picked under a binocular microscope. Kaersutite crystals and crystal fragments were picked from the magnetic 250-149 μm and 149-74 μm fractions of the gabbro and the ultramafic dyke, respectively. Biotite and alkali feldspar phenocrysts from the trachyte sample were selected from the non-magnetic 500-250 μm size fraction. A total amount of *ca*. 30 mg was concentrated for each selected mineral phase and cleaned using alcohol.

All samples, coupled with Fish Canyon sanidine neutron flux monitors and GA-1550 (MD2) biotite as secondary standards, were wrapped in aluminum foil, sealed in a quartz vial and irradiated for 14 hours in the OSU TRIGA reactor. Two individual grains from each sample were loaded into copper disks, baked-out at ~200°C for ~12-24 hours, and subsequently individually heated incrementally with an Ar-ion laser with a 2 mm defocused beam diameter. The released Ar gas was cleaned with two C-50 getters and analyzed for Ar isotopes in a MAP215-50 mass spectrometer. Analytical and data collection protocols are described in detail by Deino and Potts (1990) and Vasconcelos *et al*. (2002). Raw data were corrected for mass discrimination, nucleogenic interferences and atmospheric contamination, considering a $^{40}Ar/^{36}Ar$ ratio of 298.6 ± 0.3 in atmospheric Ar (Lee *et al*. 2006). Plateau ages are reported according to the definition of Fleck *et al*. (1977) and the integrated ages represent the combined results from all steps. We also drew inverse isochron diagrams to estimate the ^{40}Ar excess in the initial atmospheric $^{40}Ar/^{36}Ar$.

The ages are reported at a 95% confidence level using the decay constants of Steiger and Jäger (1977) and adopting a Fish Canyon sanidine age of 28.20 ± 0.05 Ma (Kuiper *et al*. 2008). The average results for the two aliquots from the internal standard GA1550 (MD-2), with proposed ages of 98.50±0.50 Ma (McDougall and Wellman 2011) or 99.44 ± 0.17 (Jourdan and Renne 2007), yielded plateau ages of 99.66± 0.51 and 99.84 ± 0.50 Ma. For comparison purposes, $^{40}Ar/^{39}Ar$ ages previously obtained by Enrich's (2005) were corrected for the new ages proposed for the $^{40}Ar/^{39}Ar$ ages by Kuiper *et al*. (2008).

SAMPLE SETTING AND RESULTS

General geology of the studied area

The main geological features of the Frade region (southwestern São Sebastião Island) have been described by Giraldo-Arroyave (2020) and are summarized in Fig. 2A. Three main major geological units crop out: the metamorphic and granitoid country rocks from the Costeiro Complex; the layered mafic-ultramafic complex; and the southern part of the São Sebastião Massif, made up mainly of alkali feldspar syenites and quartz syenites. Late ultramafic and felsic dykes cutting across the alkaline plutonic rocks were also mapped and represented in Figs. 2B and 2C.

The 380 m thick mafic-ultramafic layered sequence has a semi-circular outline, contouring the São Sebastião Massif, covering an area of approximately 8 km^2 (Fig. 2A). Medium- to coarse-grained mesocratic gabbroic rocks are predominant. Based on textural and modal properties, the intrusive rock was subdivided into four main stratigraphic levels (Giraldo-Arroyave 2020): Lower Gabbro Sequence (LGS), Intermediate Gabbro Sequence (IGS), Upper Gabbro Sequence (UGS), and Massive Leucogabbros (MLG), at around 40, 120, 140 and 30 m average thickness, respectively. Structures typical of layered complexes, as modal and graded layering, crossbedding, angular unconformities, as well as lateral grading are better developed in the lower and intermediate sequences (Fig. 3A). The predominant structure in these zones is a modal layering, given by 1 to 10 cm thick alternating plagioclase- and clinopyroxene-rich layers; olivine and apatite join clinopyroxene as cumulus phases and amphibole, Fe-Ti oxides and biotite are the main intercumulus mineral in the mafic-rich layers. Towards the top of the complex, the gabbros display mainly a subtle to moderate mineral lamination due to the orientation of the tabular plagioclase and the prismatic clinopyroxene crystals; apatite, kaersutitic amphibole and biotite are relatively scarce in the intercumulus phases. All studied samples from the intrusion are foid-absent and their alkaline character is registered in the occurrence of kaersutitic amphibole, Ti-bearing augite and Mg-rich biotite. Clinopyroxene thermobarometry suggest emplacement pressures of 0.9 ± 0.4 kbar.

The contacts between the intrusive sequence and the country rocks vary from discordant to locally concordant and, in a few sites where they were seen, detailed petrographic analysis show granophyric intergrowths of alkali feldspar and quartz in equilibrium with orthopyroxene in the matrix of the porphyritic granodiorite and a thin layer of hybrid quartz-bearing gabbros along the contact zones between the Lower Gabbro Sequence and the host granodiorite. This is evidence of high-temperature metamorphic imprint and partial melting of the country rocks as well as their partial assimilation by the intrusive magma due to shallow intrusion. Clinopyroxene barometry suggests emplacement pressures of 0.9 ± 0.4 kbar (Giraldo-Arroyave 2020).

The dark green to grayish alkali feldspar syenites from the São Sebastião Massif are medium to coarse-grained, and they are made up of alkali feldspar, clinopyroxene, calcic- and minor sodic-calcic amphibole, biotite, and accessories as fayalitic

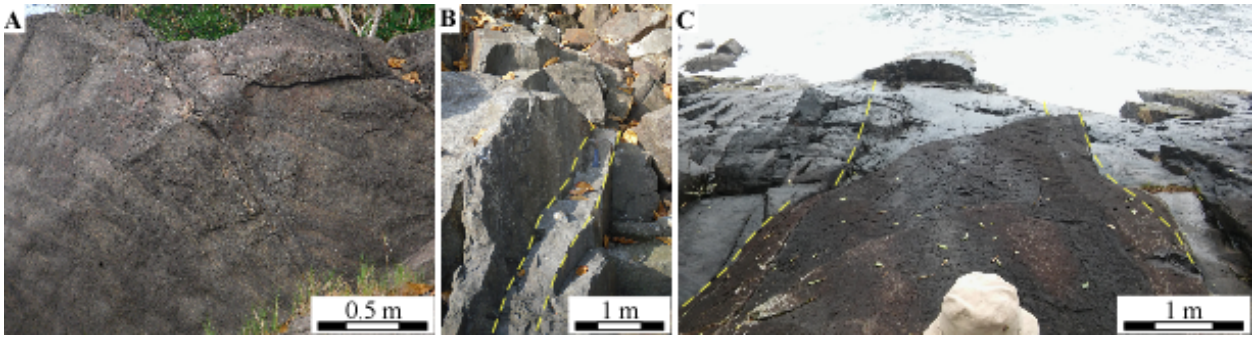

Figure 3. (A) Cross-bedding layering at the base of the sequence (LGS) with fine scale rhythmic modal layering (N30°W/30°-45°NE) given by the alternation of medium- to coarse-grained pyroxene-rich and plagioclase-rich; (B) Porphyritic picrite (N60°-75°E/90°) with a thickness of ~0.5 m; (C) Dike of a porphyritic trachyte (N70°E/90°) with a thickness of ~4 m.

olivine, quartz, opaques, chevkinite, pyrochlore and thorite (cf. Augusto 2003). Geological evidence (e.g., contact outlines, mafic xenoliths within syenites, alkali feldspar-rich dykes cross cutting the gabbro sequence near contact areas) demonstrates that the syenites are younger than the layered mafic sequence. In fact, the late emplacement of the São Sebastião Massif was responsible for the observed ring-like outline of the mafic-ultramafic sequence.

Mafi-ultramafic and felsic dykes trending 60°-75°E/90°, including microgabbros, lamprophyres, micro clinopyroxenites, micro peridotites (Fig. 3B) and porphyritic trachytes (Fig. 3C) represent the latest magmatic events in the area.

Petrography and mineralogy

A brief petrographic description and characterization of the minerals chosen for $^{40}Ar/^{39}Ar$ dating are given in the following.

Olivine-Bearing Kaersutite Gabbro

Sample IBI-2e is representative of a ca. 2-5 m layer of well-laminated and layered orthocumulates of the Intermediate Gabbro Sequence (IGS) (Fig. 3A), comoprising plagioclase (39 vol. %), clinopyroxene (19%), amphibole (14%), FeTi-oxides (10%), olivine (7%), apatite (6%) and biotite (5%). Oriented plagioclase and clinopyroxene crystals constitute the main cumulus rock framework (Fig. 4A) accompanied by prismatic apatite and sub-equant olivine. Plagioclase crystals (1-8 mm) are euhedral, tabular, Albite-Carlsbad twinned, compositionally homogeneous, and correspond to a labradorite. Clinopyroxene (up to 4 mm) is pale pink, prismatic, subhedral and corresponds to an alumina augite (Morimoto *et al.* 1988). Olivine is also homogeneous, usually subhedral with an average grain size of ~ 1 mm and occasionally appears partially substituted by symplectitic intergrowths of dendritic magnetite and pyroxene. The Fe-Ti oxides are ilmenite and magnetite and appear as intercumulus material. Apatite occurs as euhedral prismatic crystals lying along the main rock lamination. The main intercummulus phases are calcic-amphibole and minor biotite. The amphibole typically forms *oikocrysts* enclosing *chadacrysts* of plagioclase, olivine, pyroxene, apatite and Ti-Fe oxides; it also appears as thin rims overgrowing clinopyroxene crystals (Figs. 4A and 4B). It is subhedral to anhedral and pleochroic (light to reddish-brown), as typical for kaersutites. Biotite is subhedral, with pale to reddish-brown pleochroic colors.

Representative amphibole compositions are shown in Tab. 1 and illustrated in Fig. 5A. Overall, the amphibole is relatively homogeneous and can be classified as ferri-kaersutite according to Leake *et al.* (1997) ($^{IV}Al > 1.5$, $Ti\ ^{3}\ 0.5$ and $(Na+K) > 0.5$ apfu) (see also Hawthorne *et al.* 2012). Magnesium number [mg#= $(Mg/(Mg + Fe^{2+})$] ranges from of 0.70 to 0.74, with average content (wt%) of FeO^{T}, Al_2O_3 and TiO_2 at 11.9, 12.4 and 4.8, respectively. F and Cl abundances are low, up to 0.16 and 0.04 wt. %, respectively.

Porphyritic Picrite

It crops out as a 0.5 m thick subvertical dyke running N60°E (Fig. 3B) and shows a distinct lateral zoning: in the core, from where sample IBI-06f was collected, it has a porphyritic texture with 18 vol. % macrocrysts in a fine grained mesostasis (82 vol. %); at the external contacts with the main gabbro, thin chilled margins (up to 0.5 cm) with fine-grained to aphanitic textures can be observed.

Modal composition is olivine (31 vol. %), clinopyroxene (30%), plagioclase (9%), kaersutite (9%), FeTi-oxides (8%), calcite (5%) and biotite (*ca.* ~1%). The texture is characterized by subhedral to anhedral macrocrysts (> 2 mm) to microcrysts (> 0.5 mm) of olivine and zoned clinopyroxene (Figs. 4C and 4D). The larger olivine and clinopyroxene crystals show irregular or curved outlines, large embayments and were partially replaced by chlorite and/or calcite. The mesostasis is fine-grained and composed of olivine, pyroxene (aluminian diopside to augite) (Morimoto *et al.* 1988) labradoritic plagioclase laths, Fe-Ti oxides, and small amounts of euhedral to subhedral kaersutite, containing some euhedral apatite inclusions, minor biotite and calcite.

Representative chemical compositions for the kaersutite is shown in Tab. 1 and plotted in Fig. 5A. It classifies as ferri-kaersutite (Leake *et al.* 1997, Hawthorne *et al.* 2012) and, compared with the ferri-kaersutite from the host gabbro, it shows similar mg# values (0.68 to 0.70) but distinctively higher TiO_2 and Al_2O_3 contents (up to 6.4 and 15.4 wt%, respectively) and somewhat higher Na_2O and F, up to 2.6 and 0.22 (wt%) respectively.

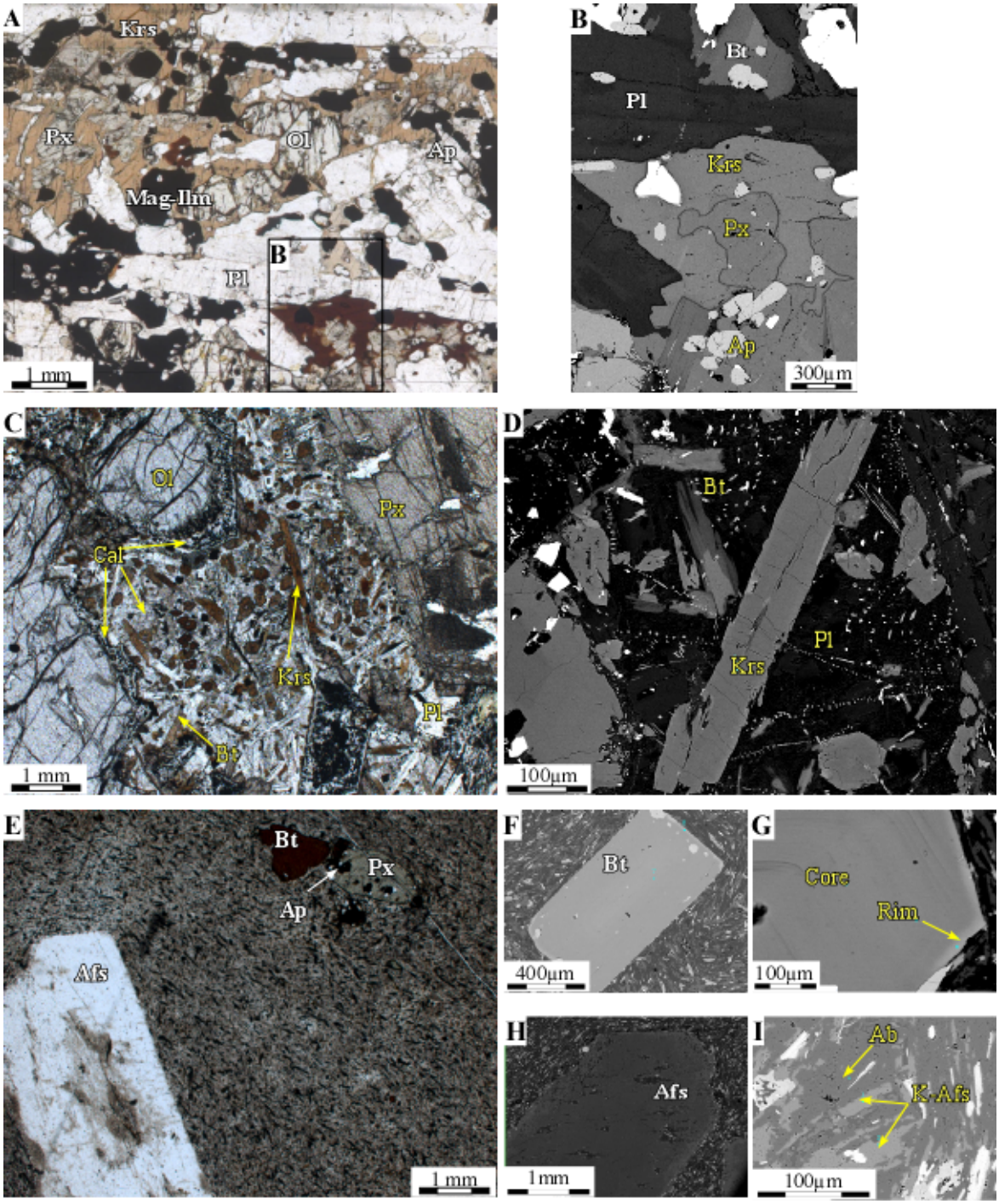

Figure 4. Plane-polarized light (PPL) image of olivine-bearing kaersutite gabbro (IBI-2e). (A) Plagioclase (Pl), pyroxene (Px), olivine (Ol) and apatite (Ap) with intercumulus kaersutite (Krs) and magnetite-ilmenite (Mag-Ilm); (B) back-scattered electron (BSE) image of kaersutite rimming pyroxene, detail of image A; (C) PPL image of olivine basalt dike (IBI-6g). Macrocryst of olivine (Ol) and clinopyroxene (Px) set in a groundmass of olivine, pyroxene, plagioclase and small amounts of kaersutite and biotite, calcite and magnetite; (D) BSE image of groundmass kaersutite; € PPL image of trachyte with flow alignment of euhedral phenocryst of sanidine, biotite and pyroxene and groundmass composed of almost pure orthoclase and albite; (F) BSE image of zoned euhedral biotite with some apatite inclusions; (G) Detail BSE image of zoned biotite phenocryst; (H) BSE image of alkali feldspar phenocryst; (I) Albite and K-feldspar in the groundmass.

Porphyritic Trachyte

The IBI-06a sample is representative of a 4 m thick subvertical dyke striking N70°E, sub parallel to the porphyritic picrite (Fig. 3C). The rock shows a well-developed magmatic foliation parallel to its walls, containing up to 13 vol% phenocrysts [alkali feldspar (8 %), biotite (4 %), and clinopyroxene (1 %)] and 87 vol% of a fine-grained mesostasis (Figs. 4E–4I). Alkali feldspar phenocrysts (up to 10 mm) are euhedral, tabular and Carlsbad twinned. Crystals are mostly clean and transparent under transmitted light, without evidence suggesting exsolution lamellae; however, some crystal rims and internal patches are cloudy and suggest some subsolidus imprint. Biotite (up to 2 mm) is euhedral to subhedral and shows brown to reddish pleochroism. The clinopyroxene is a relatively homogeneous augite It occurs as 0.2 to 0.5 mm euhedral crystals with slightly pleochroic green colors. The mesostasis is mainly composed

Table 1. Representative chemical analyses (wt. %) of selected minerals from the layered gabbro and the cross cutting porphyritic picrite and trachyte dykes.

	IBI-2e	IBI-06f	IBI-06a					
			Bt-c	Bt-r	Bt-m	Afs	Afs-m1	Afs-m2
SiO_2	41.50	38.46	36.07	36.56	34.48	65.77	69.30	65.79
TiO_2	4.85	6.28	6.51	4.61	5.53	0.05	0.02	0.00
Cr_2O_3	0.00	0.01						
Al_2O_3	12.42	13.90	13.87	13.33	12.25	20.08	19.92	19.00
FeO	11.94	12.12	16.34	22.23	28.03			
Fe_2O_3						0.21	0.14	0.11
MnO	0.17	0.17	0.48	1.21	1.46	0.00	0.00	0.01
MgO	13.07	12.17	12.48	8.00	4.90	0.01	0.01	0.01
ZnO	0.02	0.01						
CaO	11.14	11.14	0.02	0.41	0.06	0.87	0.02	0.03
Na_2O	2.36	2.48	0.84	0.51	0.60	6.28	10.94	0.31
K2O	1.26	1.07	8.25	7.74	8.44	6.60	0.42	14.83
SrO						0.07	0.03	0.01
BaO			0.45	0.03	0.02	0.14	0.00	0.01
F	0.13	0.23	0.35	0.13	0.11			
Cl	0.02	0.02	0.04	0.04	0.03			
O=F=Cl	0.06	0.10	0.16	0.06	0.05			
Total	98.80	97.96	95.54	94.73	95.86	100.07	100.79	100.11
mg#	0.72	0.70	0.58	0.39	0.24			
An (Ca)						4.33	0.09	0.15
Ab (Na)						56.55	97.42	3.09
Or (K)						39.12	2.48	96.76

Krs: kaersutite; Afs: Alkali feldspar; Bt: Biotite; c: core; r: rim; m1: groundmass albite; m2: groundmass alkali feldspar.

of alkali feldspar (K-feldspar and albite) laths, which impart a trachytic-like texture to the rock, and small quantities of biotite and accessory minerals (mainly apatite and magnetite). No quartz or feldspathoid were observed, indicating crystallization close to SiO_2-saturation conditions.

Representative compositions for biotite and alkali feldspar are listed in Tab. 1; in the case of the alkali feldspar phenocrysts, we also obtained an X-ray diffraction pattern for the most transparent crystal fragments to characterize its structural state.

The biotite phenocrysts are compositionally zoned (Fig. 5B). The core corresponds to a Mg-biotite ($Ann_{27}Ph_{50}Sid_{23}$) (Rieder *et al.* 1998), with mg# values averaging 0.58 and relatively high TiO_2 contents (up to 7.5 wt%); BaO ranges from 0.08 to 1.7 and F from 0.25 to 0.42 wt%. The annite component in the biotite increases towards the crystal rims, averaging $Ann_{41}Ph_{33}Sid_{26}$, accompanied by a decrease in TiO_2 (2.8 to 5.7 wt%), mg # (up to 44%), BaO (≤ 0.05 wt%.) and F (≤ 0.16 wt%). Biotite crystals in the groundmass correspond to annite ($Ann_{40\text{-}70}Ph_{13\text{-}31}Sid_{34\text{-}17}$) with TiO_2 contents up to 6.0 wt%, and 14 ≤ mg# ≤ 36, BaO ≤ 0.04 and F ≤ 0.14 wt%.

The alkali feldspar phenocrysts have homogenous compositions, averaging $Ab_{57}Or_{39}An_4$ (Fig. 5C), with $Fe_2O_3^T$ up to 0.22 wt. % and relatively low contents of both BaO (≤ 0.12 wt. %) and SrO (≤ 0.06 wt%). The mesostasis contains almost pure K-feldspar ($Or_{97}Ab_3$) and albite ($Ab_{99}Or_1$) laths. The X-ray diffraction pattern for pristine phenocryst fragments (Fig. 5D) reveals an almost homogenous structure, with well-developed and single (130) and (131) diffraction peaks, typical of a disordered monoclinic phase.

Given the diffraction pattern and the chemical composition, it corresponds to a homogeneous high-Na sanidine.

$^{40}Ar/^{39}Ar$ results

Analytical results from the step-heating experiments are summarized in Tab. 2 and illustrated in Figs. 6 and 7. Argon release age, K/Ca spectra, inverse isochrons and probability density plots are shown for each sample.

Olivine-Bearing Kaersutite Gabbro

In this sample, the two kaersutite aliquots contained nine crystals or crystal fragments. Both aliquots yield compatible plateau ages of 87.9 ± 0.8 Ma and 88 ± 1 Ma, represented by more than 78% of the Ar released over eight consecutive steps (Fig. 6A). Slightly older ages are observed in the low-temperature steps due to small excess Ar components, resulting in somewhat older integrated ages of ~ 91 Ma. The K/Ca ratios are nearly constant (~ 0.1) as cumulative % ^{39}Ar released increases. The inverse $^{36}Ar/^{40}Ar$ *vs.* $^{39}Ar/^{40}Ar$ correlation diagram yields

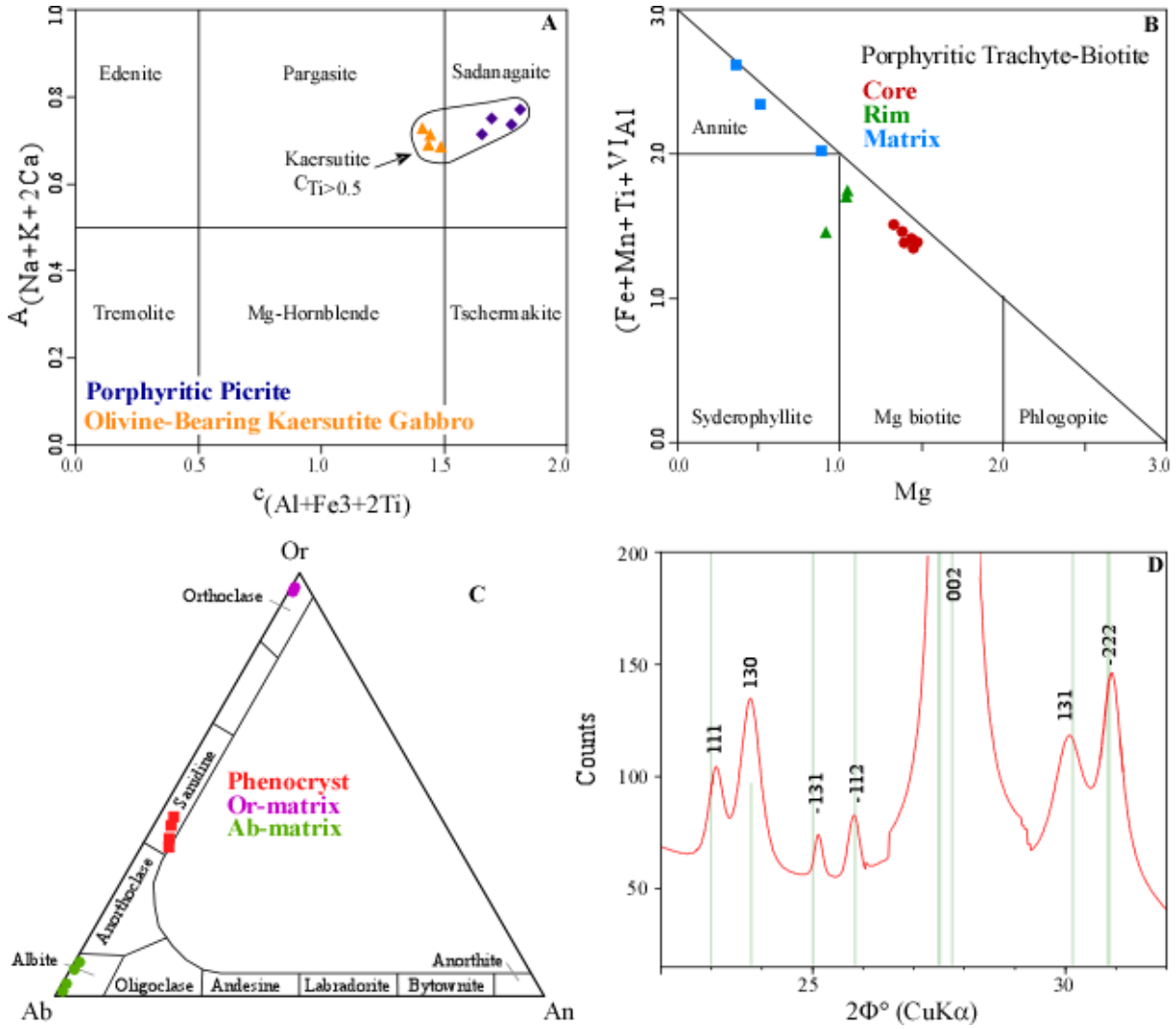

Figure 5. Classification diagram and X-ray powder pattern for the dated minerals. (A) amphiboles of the olivine-bearing kaersutite gabbro and porphyritic picrite; (B) biotite phenocrysts of the porphyritic trachyte; (C) alkali feldspar phenocrysts and groundmass alkali feldspars; (D) partial X-Ray powder diffraction for alkali feldspar phenocrysts. See text.

an isochron that defines an age of 87.1 ± 1.3 Ma; the $^{40}Ar/^{39}Ar$ atmospheric ratio (480 ± 290) is poorly constrained (Fig. 6B) but it suggests some excess argon in the sample. The probability density plot for the plateau steps of both aliquots peaks at 87.7 Ma and yields a weighted mean age of 87.9 ± 0.7 Ma (MSWD = 0.76, Probability = 0.68), in agreement with the plateau ages, and that is herein considered the best age estimate.

Porphyritic Picrite

Two aliquots, also made up of nine kaersutite crystals or crystal fragments, were analyzed for this sample. One aliquot yielded a plateau age of 86.5 ± 1.3 Ma, defined by the release of ~ 54% of ^{39}Ar in three consecutive steps. Excess ^{40}Ar was observed in both lower and higher temperature steps, yielding a saddle-shaped spectrum that defines an older integrated age of 93.4 ± 1.3 Ma. The second aliquot yielded a relatively undisturbed spectrum with a plateau age of 86.0 ± 0.8, containing > 90% of the released ^{39}Ar over ten consecutive steps. In both cases, the K/Ca ratios vary in the lowest and highest temperature steps (~ 0.8 and ~ 0.02, respectively) (Fig. 6C). The inverse isochron is well defined, and it defines an age of 85.8 ± 1.2 Ma, with a $^{40}Ar/^{39}Ar$ value of 313 ± 41, compatible with the expected atmospheric Ar value (Fig. 6D). The probability density plot for all plateau steps peaks at 85.9 Ma, with a weighted mean age of 86.0 ± 0.8 Ma (MSWD = 0.58, Probability = 0.85), which is considered the best age estimate for the sample.

Porphyritic Trachyte

Two biotite and two alkali feldspar aliquots, each constituted by single phenocrysts or phenocryst fragments were analyzed.

The biotite aliquots yielded similar Ar release spectra, integrating more than 95% of the gas released. Aliquot one shows a ten-step plateau age of 86.0 ± 0.5 Ma, a value identical to the integrated age. The results for the second aliquot are almost identical, with 86.2 ± 0.5 and 86.0 ± 0.5 Ma for the plateau (9 steps) and the integrated ages (Fig. 7A), respectively. Large variations are observed for the K/Ca ratios in both aliquots, pointing to relatively inhomogeneous biotite compositions, in agreement with our chemical data. The corresponding isochron plot for all plateau steps defines an age of 86.2 ± 0.5 Ma, with $^{40}Ar/^{36}Ar$ value of 284 ± 39 Ma (Fig. 7B). The probability density plot, integrating the steps of both aliquots, shows a probability peak at 86.1 and a weighted mean age of 86.1 ± 0.5 Ma (MSWD = 1.7, Probability = 0.5).

Table 2. $^{40}Ar/^{39}Ar$ analytical results for aliquots 01 and 02 of the dated mineral phases from the layered gabbro (IBI-2e), the porphyritic picrite (IBI-06f) and the porphyritic trachyte (IBI-06a). Data are sorted with increasing heating step. Errors are given in 1s.

Sample-Run ID	$^{40}Ar/^{39}Ar$	$^{36}Ar/^{39}Ar$	$^{37}Ar/^{39}Ar$	$^{40}Ar^*/^{39}Ar$	%Ar40*	%Ar40* (1s)	Age (Ma)	Age Ma (± 1s)	Ar^{40} (moles)	J	J (± 1s)
IBI-02e (Amphibole)											
IBI2e-01A	67.3507	2.66E-02	-6.89E-01	59.3362	88.1434	11.8934	367.348	87.005	3.45E-15	0.00381	9.00E-06
IBI2e-01B	13.0918	-7.80E-02	8.85E+00	37.2665	282.9327	173.613	239.289	173.542	2.79E-16	0.00381	9.00E-06
IBI2e-01CA	52.3504	-8.13E-02	2.19E+00	76.8653	146.6082	72.79877	462.956	286.608	1.11E-15	0.00381	9.00E-06
IBI2e-01D	210.4013	2.86E-01	4.37E+00	125.7340	59.5787	8.09227	705.498	228.228	5.59E-15	0.00381	9.00E-06
IBI2e-01E	16.8774	3.98E-03	4.20E+00	16.0568	94.8666	2.583011	107.014	3.135	1.87E-14	0.00381	9.00E-06
IBI2e-01F	13.4783	1.83E-03	3.82E+00	13.2602	98.1281	0.6259631	88.826	0.656	8.54E-14	0.00381	9.00E-06
IBI2e-01G	13.1896	1.70E-03	3.84E+00	13.0115	98.3942	0.5864764	87.199	0.584	9.47E-14	0.00381	9.00E-06
IBI2e-01H	13.2645	1.64E-03	3.86E+00	13.1039	98.5316	0.612563	87.803	0.650	1.01E-13	0.00381	9.00E-06
IBI2e-01I	14.7494	6.68E-03	3.73E+00	13.0734	88.4130	13.30444	87.604	13.259	3.49E-15	0.00381	9.00E-06
IBI2e-01J	13.7666	1.87E-03	4.09E+00	13.5585	98.2162	5.241094	90.774	4.942	8.45E-15	0.00381	9.00E-06
IBI2e-01K	13.8852	3.26E-03	3.94E+00	13.2501	95.1713	5.124746	88.760	4.755	1.08E-14	0.00381	9.00E-06
IBI2e-01L	15.9323	8.03E-03	5.80E+00	14.0347	87.7409	3.912265	93.881	4.289	1.18E-14	0.00381	9.00E-06
IBI2e-02A	74.5484	8.84E-02	4.48E+00	48.6492	65.0574	2.301248	306.471	13.597	2.09E-14	0.00381	9.00E-06
IBI2e-02B	14.2077	2.38E-03	3.81E+00	13.8242	97.0501	0.7327117	92.509	0.776	7.49E-14	0.00381	9.00E-06
IBI2e-02C	13.4082	2.41E-03	3.64E+00	12.9991	96.7116	1.233526	87.119	1.163	3.91E-14	0.00381	9.00E-06
IBI2e-02D	13.3060	1.93E-03	4.04E+00	13.0736	97.9857	0.5668716	87.606	0.537	1.09E-13	0.00381	9.00E-06
IBI2e-02E	13.2088	9.90E-04	3.67E+00	13.2273	99.8925	1.075132	88.611	1.032	4.21E-14	0.00381	9.00E-06
IBI2e-02F	13.2393	8.05E-04	3.35E+00	13.2864	100.1288	0.9602797	88.997	0.927	4.55E-14	0.00381	9.00E-06
IBI2e-02G	14.0341	-2.26E-03	3.44E+00	15.0071	106.6854	6.813946	100.208	6.573	6.50E-15	0.00381	9.00E-06
IBI2e-02H	14.2621	-3.70E-03	3.06E+00	15.6340	109.3939	9.593799	104.276	9.214	5.01E-15	0.00381	9.00E-06
IBI2e-02I	13.0866	1.50E-05	2.46E+00	13.2916	101.4003	9.628881	89.031	8.317	6.28E-15	0.00381	9.00E-06
IBI2e-02J	13.5826	4.96E-03	3.75E+00	12.4191	91.2027	5.473919	83.320	5.020	9.12E-15	0.00381	9.00E-06
IBI2e-02K	18.1585	5.93E-02	8.06E+00	1.0828	5.9300	69.762	7.419	87.116	6.64E-16	0.00381	9.00E-06
IBI-06a (Biotite)											
IBI06a-01A	17.7477	2.47E-02	8.16E-02	10.3697	58.4280	4.197531	69.833	5.057	1.11E-14	0.00381	9.00E-06
IBI06a-01B	14.7244	7.42E-03	-2.70E-02	12.5051	84.9342	1.181141	83.883	1.244	4.11E-14	0.00381	9.00E-06
IBI06a-01C	14.2238	4.13E-03	6.06E-02	12.9955	91.3662	0.6117821	87.095	0.646	8.18E-14	0.00381	9.00E-06
IBI06a-01D	13.3159	1.28E-03	5.73E-03	12.9337	97.1349	0.584821	86.690	0.588	8.81E-14	0.00381	9.00E-06
IBI06a-01E	13.3077	1.69E-03	2.28E-02	12.8034	96.2146	0.4424589	85.837	0.423	1.26E-13	0.00381	9.00E-06
IBI06a-01F	13.2626	1.35E-03	4.16E-03	12.8599	96.9699	0.4585215	86.208	0.446	1.06E-13	0.00381	9.00E-06

Continue...

Table 2. Continuation.

Sample-Run ID	$^{40}Ar/^{39}Ar$	$^{36}Ar/^{39}Ar$	$^{37}Ar/^{39}Ar$	$^{40}Ar^*/^{39}Ar$	%Ar40*	%Ar40* (1s)	Age (Ma)	Age Ma (± 1s)	Ar^{40} (moles)	J	J (± 1s)
IBI06a-01G	13.2937	1.49E-03	2.67E-02	12.8515	96.6778	0.4344391	86.152	0.459	1.40E-13	0.00381	9.00E-06
IBI06a-01H	13.1106	8.75E-04	1.30E-02	12.8497	98.0151	0.2020562	86.141	0.236	3.76E-13	0.00381	9.00E-06
IBI06a-01I	13.1175	1.18E-03	1.64E-02	12.7659	97.3240	0.2034505	85.592	0.222	3.30E-13	0.00381	9.00E-06
IBI06a-01J	13.1695	9.80E-04	-1.57E-02	12.8747	97.7684	0.85134	86.304	0.820	5.48E-14	0.00381	9.00E-06
IBI06a-01K	13.3998	4.12E-03	1.70E-01	12.1828	90.9128	6.734606	81.770	6.161	6.64E-15	0.00381	9.00E-06
IBI06a-02A	12.9447	1.44E-02	3.55E-01	8.6648	66.9249	3.632063	58.535	3.190	1.43E-14	0.00381	9.00E-06
IBI06a-02B	13.6851	3.22E-03	7.26E-02	12.7295	93.0177	0.6263542	85.353	0.651	8.90E-14	0.00381	9.00E-06
IBI06a-02C	13.0474	2.50E-04	2.12E-02	12.9737	99.4396	0.3491518	86.952	0.380	1.65E-13	0.00381	9.00E-06
IBI06a-02D	13.0791	5.36E-04	3.80E-02	12.9214	98.7978	0.3577191	86.610	0.375	1.76E-13	0.00381	9.00E-06
IBI06a-02E	13.1169	4.98E-04	1.59E-02	12.9687	98.8752	0.2848899	86.919	0.337	1.98E-13	0.00381	9.00E-06
IBI06a-02F	13.0350	4.96E-04	3.71E-02	12.8893	98.8857	0.2957916	86.400	0.363	1.87E-13	0.00381	9.00E-06
IBI06a-02G	12.9558	4.08E-04	1.18E-02	12.8342	99.0663	0.2903061	86.039	0.316	2.16E-13	0.00381	9.00E-06
IBI06a-02H	12.9299	4.37E-04	2.66E-02	12.8009	99.0064	0.1885498	85.821	0.230	3.53E-13	0.00381	9.00E-06
IBI06a-02I	12.9814	4.86E-04	4.23E-02	12.8392	98.9077	0.1351966	86.072	0.212	5.56E-13	0.00381	9.00E-06
IBI06a-02J	13.0694	-5.47E-04	4.72E-01	13.2722	101.5251	4.039879	88.904	3.624	1.28E-14	0.00381	9.00E-06
IBI06a-02K	13.2697	-1.72E-03	-4.86E-01	13.7397	103.5828	6.338945	91.957	5.835	6.51E-15	0.00381	9.00E-06
IBI06a-02L	14.1854	7.09E-04	1.13E+00	14.0730	99.1355	33.17047	94.131	31.286	1.40E-15	0.00381	9.00E-06
IBI-06a (Alkali Feldspar)											
IBI06a-01A	61.6794	1.85E-02	-5.30E+00	55.4942	90.3030	66.30333	345.698	333.030	6.31E-16	0.00381	9.00E-06
IBI06a-01B	24.6258	-3.03E-04	-4.81E+00	24.2651	98.8660	21.8024	159.361	36.066	1.98E-15	0.00381	9.00E-06
IBI06a-01C	12.8229	2.55E-04	4.44E-02	12.7498	99.4334	0.9628391	85.486	0.898	5.37E-14	0.00381	9.00E-06
IBI06a-01D	12.7797	1.43E-04	-1.25E-02	12.7352	99.6586	1.049572	85.391	0.913	8.26E-14	0.00381	9.00E-06
IBI06a-01E	12.8929	4.55E-04	-6.28E-02	12.7509	98.9085	0.6852983	85.493	0.639	6.67E-14	0.00381	9.00E-06
IBI06a-01F	12.6843	4.75E-04	8.08E-02	12.5486	98.9304	1.54124	84.168	1.324	5.12E-14	0.00381	9.00E-06
IBI06a-01G	13.0728	5.55E-04	5.88E-02	12.9114	98.7672	0.7206254	86.544	0.687	6.49E-14	0.00381	9.00E-06
IBI06a-01H	12.9576	1.87E-04	7.30E-02	12.9072	99.6118	0.5630071	86.517	0.558	8.06E-14	0.00381	9.00E-06
IBI06a-01I	12.9901	1.99E-04	3.68E-02	12.9330	99.5643	0.4557366	86.686	0.483	1.09E-13	0.00381	9.00E-06
IBI06a-01J	13.0991	7.96E-04	1.47E-02	12.8620	98.1953	0.6955211	86.221	0.662	6.95E-14	0.00381	9.00E-06
IBI06a-01K	12.8503	2.65E-04	4.38E-02	12.7741	99.4096	0.2051513	85.645	0.272	2.88E-13	0.00381	9.00E-06
IBI06a-02A	103.8276	6.84E-02	3.26E-02	83.3954	80.3198	0.7580457	497.316	8.124	8.04E-14	0.00381	9.00E-06
IBI06a-02B	17.7125	3.85E-03	7.26E-02	16.5691	93.5446	0.3678833	110.326	0.578	1.59E-13	0.00381	9.00E-06

Continue...

Table 2. Continuation.

Sample-Run ID	$^{40}Ar/^{39}Ar$	$^{36}Ar/^{39}Ar$	$^{37}Ar/^{39}Ar$	$^{40}Ar^*/^{39}Ar$	%Ar40*	%Ar40* (1s)	Age (Ma)	Age Ma (± 1s)	Ar^{40} (moles)	J	J (± 1s)
IBI06a-02C	12.6817	6.69E-04	6.86E-02	12.4870	98.4665	0.2567351	83.764	0.273	2.49E-13	0.00381	9.00E-06
IBI06a-02D	12.6559	5.63E-04	8.20E-02	12.4940	98.7212	0.3496216	83.810	0.371	1.71E-13	0.00381	9.00E-06
IBI06a-02E	13.0597	1.72E-03	6.40E-02	12.5521	96.1155	0.5163789	84.192	0.545	9.25E-14	0.00381	9.00E-06
IBI06a-02F	13.8392	2.24E-03	7.56E-02	13.1750	95.2012	0.7977173	88.269	0.820	6.57E-14	0.00381	9.00E-06
IBI06a-02G	14.5864	1.61E-03	7.37E-02	14.1118	96.7468	0.397542	94.383	0.483	1.31E-13	0.00381	9.00E-06
IBI06a-02H	14.6374	1.67E-03	6.82E-02	14.1441	96.6309	0.3789717	94.594	0.483	1.49E-13	0.00381	9.00E-06
IBI06a-02I	14.5389	1.24E-03	7.83E-02	14.1749	97.4966	0.3880369	94.795	0.474	1.44E-13	0.00381	9.00E-06
IBI06a-02J	14.4446	1.91E-03	8.72E-02	13.8822	96.1063	0.5467809	92.887	0.620	9.73E-14	0.00381	9.00E-06
IBI06a-02K	14.1446	1.24E-03	7.33E-02	13.7801	97.4233	0.1252567	92.221	0.189	1.35E-12	0.00381	9.00E-06
IBI-06f (Amphibole)											
IBI06f-01A	45.5497	7.91E-02	1.11E+00	22.0385	48.3469	1.418086	145.311	4.564	4.66E-14	0.00381	9.00E-06
IBI06f-01B	18.6388	1.47E-02	2.34E+00	14.4489	77.3985	1.358763	96.579	1.750	4.09E-14	0.00381	9.00E-06
IBI06f-01C	16.1932	5.77E-03	2.88E+00	14.7214	90.7345	1.080325	98.351	1.291	4.51E-14	0.00381	9.00E-06
IBI06f-01D	13.9942	4.46E-03	3.35E+00	12.9483	92.3176	1.565137	86.786	1.502	5.24E-14	0.00381	9.00E-06
IBI06f-01E	13.8105	3.66E-03	3.90E+00	13.0524	94.2615	1.188517	87.467	1.139	6.61E-14	0.00381	9.00E-06
IBI06f-01F	13.6697	4.06E-03	4.12E+00	12.8106	93.4540	0.848687	85.884	0.853	6.19E-14	0.00381	9.00E-06
IBI06f-01G	14.3878	3.11E-03	3.98E+00	13.8030	95.6768	1.460889	92.370	1.487	3.58E-14	0.00381	9.00E-06
IBI06f-01H	16.3240	6.20E-03	4.33E+00	14.8474	90.6863	4.23734	99.170	4.768	1.17E-14	0.00381	9.00E-06
IBI06f-01I	22.2989	2.51E-02	4.83E+00	15.2324	68.0845	2.196394	101.671	3.405	2.48E-14	0.00381	9.00E-06
IBI06f-01J	17.2240	1.69E-02	1.91E+01	13.8230	79.2011	2.195169	92.500	2.633	2.32E-14	0.00381	9.00E-06
IBI06f-01K	17.6460	1.08E-02	2.06E+01	16.2219	90.6231	11.54715	108.082	14.094	3.49E-15	0.00381	9.00E-06
IBI06f-02A	23.1730	2.64E-02	7.76E-01	15.3704	66.2955	1.334943	102.566	2.189	3.77E-14	0.00381	9.00E-06
IBI06f-02B	15.5335	8.50E-03	1.98E+00	13.1653	84.6426	1.314044	88.205	1.435	4.42E-14	0.00381	9.00E-06
IBI06f-02C	13.5753	3.40E-03	3.02E+00	12.8179	94.2291	0.9518917	85.932	0.945	4.90E-14	0.00381	9.00E-06
IBI06f-02D	13.7040	4.45E-03	3.58E+00	12.6826	92.3224	0.7409019	85.046	0.755	6.58E-14	0.00381	9.00E-06
IBI06f-02E	13.5060	3.42E-03	4.11E+00	12.8347	94.7653	0.704291	86.042	0.694	8.41E-14	0.00381	9.00E-06
IBI06f-02F	14.1250	5.47E-03	3.90E+00	12.8247	90.5553	1.326622	85.977	1.337	3.76E-14	0.00381	9.00E-06
IBI06f-02G	14.1467	3.07E-03	4.07E+00	13.5802	95.7303	2.540449	90.916	2.504	1.98E-14	0.00381	9.00E-06
IBI06f-02H	14.3398	5.24E-03	4.07E+00	13.1233	91.2641	3.425025	87.930	3.369	1.33E-14	0.00381	9.00E-06
IBI06f-02I	13.7472	4.48E-03	4.34E+00	12.7809	92.6981	1.059696	85.690	1.062	4.42E-14	0.00381	9.00E-06
IBI06f-02J	17.1561	1.57E-02	4.00E+00	12.8041	74.4306	2.319744	85.842	2.706	2.13E-14	0.00381	9.00E-06
IBI06f-02K	32.5249	6.84E-02	4.76E+00	12.5056	38.3237	5.237783	83.886	11.513	1.00E-14	0.00381	9.00E-06

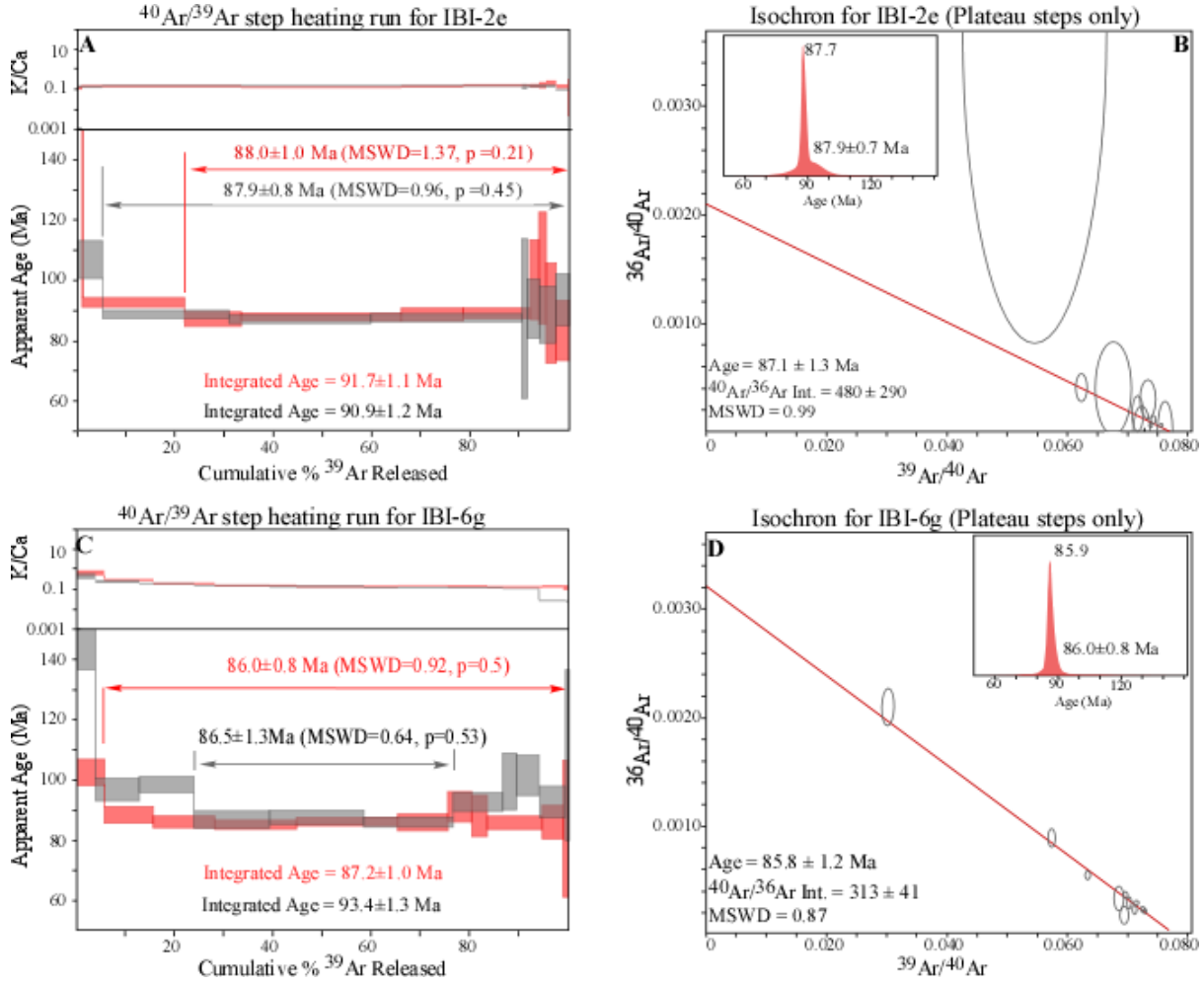

Figure 6. Age argon-release spectra, $^{36}Ar/^{40}Ar$ versus $^{39}Ar/^{40}Ar$ isochron plot and age probability (plateau only) diagrams for $^{40}Ar/^{39}Ar$ step heating experiments for kaersutite from (A and B) the olivine-bearing kaersutite gabbro and (C and D) the porphyritic picrite. See text for discussion.

One of the alkali feldspar fractions produced a highly disturbed apparent age *vs.* released ^{39}Ar, not defining a plateau, as well as a poor probability density plot with peaks at 83.7, 85.7 (strongest), 92.3 and 94.6 Ma, and therefore was not considered. These inferior results likely represent a complex distribution of noble gases in the feldspar, most likely related to post-magmatic effects. The other aliquot produced a well-defined spectrum, showing significant K/Ca variations, as expected for alkali feldspars, and release of near 100% of ^{39}Ar in nine consecutive steps. The results are 86.0 ± 0.5 and 86.0 ± 0.6 Ma for the plateau and the integrated age, respectively (Fig. 7C). The probability density diagram peaks at 85.7 and gives a weighted mean age 85.9 ± 0.5 Ma (MSWD = 1.1, Probability = 0.4).

The ages obtained for biotite and alkali feldspar from the trachyte are almost identical to those obtained for kaersutite from the porphyritic picrite, pointing to its coeval nature.

DISCUSSION

On the timing of the alkaline magmatism in the São Sebastião Island

Accepted Ar closure temperatures for the dated minerals vary from *ca.* 600°C (calcic amphiboles), to *ca.* 450°C (biotite), and down to *ca.* 300°C (alkali feldspar) (e.g., Harrison and McDougall 1981, Villa 1998, Hora *et al.* 2010). The close overlap of results for the three mineral systems suggest that the layered mafic rocks investigated here were emplaced in a relatively shallow continental crust, consistent with the pressure estimates of *ca.* 0.9 ± 0.4 kbar of Giraldo-Arroyave (2020). The similarity in ages suggest that the cross-cutting dykes must also have been emplaced at similar or shallower levels. Shallow magmatic systems cool relatively fast, and the measured ages should be close to the crystallization ages, as suggested by the nearly identical results obtained for biotite and alkali feldspar phenocrysts from the porphyritic trachyte.

Our new ages help to advance understanding of magmatism in the São Sebastião Island and neighboring areas, as they constrain the timing of the main alkaline magmatic events more precisely.

The integration of the geological and the high-precision geochronological information indicates that the first magmatic event was the emplacement of basic alkaline melts and development of the mafic-ultramafic alkaline layered intrusion at 87.9 ± 0.7 Ma. Given the geological and petrographic similarities between the northern and southern mafic-ultramafic plutonic rocks in the island, this age is tentatively extended for the emplacement of the layered mafic-ultramafic rocks in the

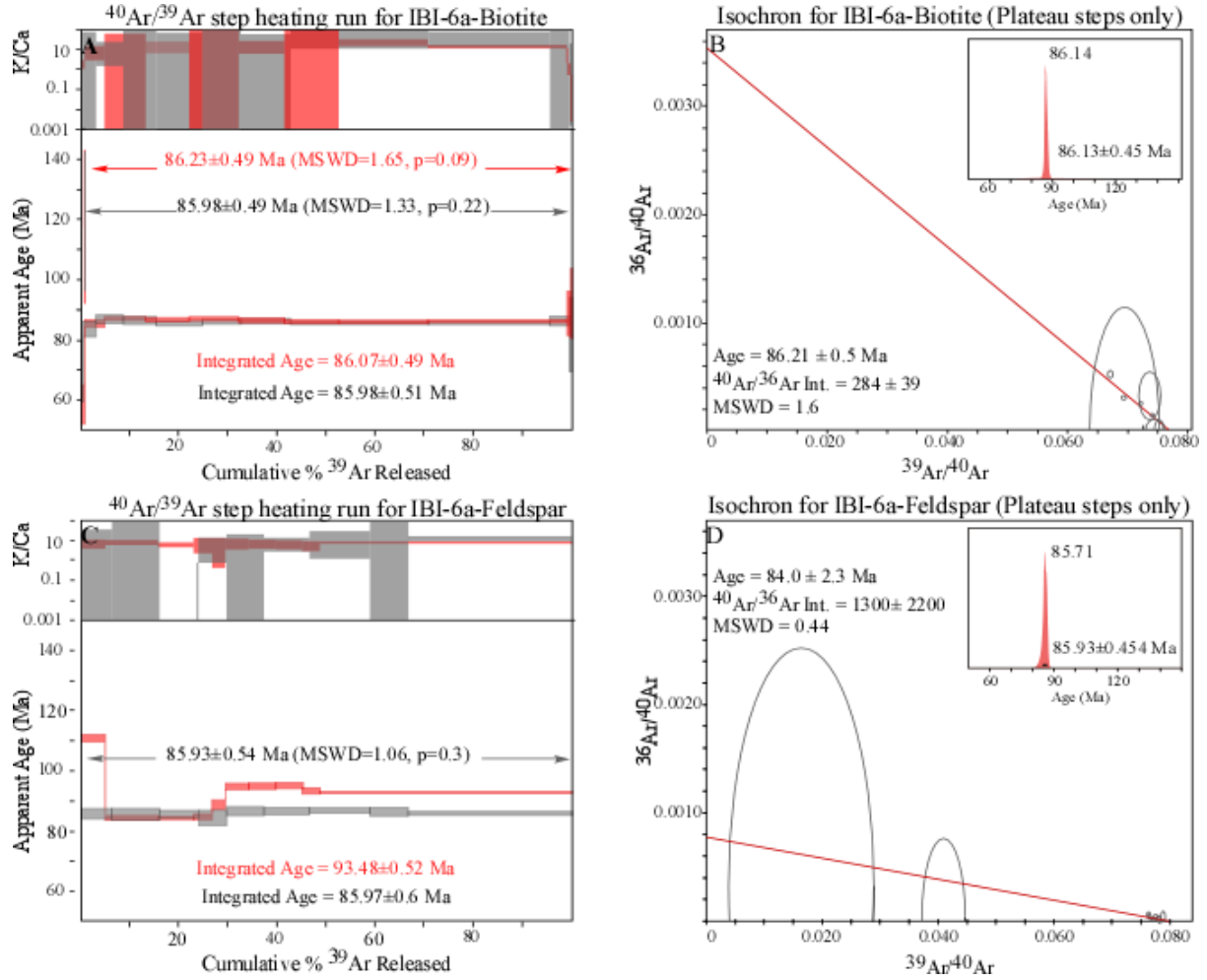

Figure 7. (A) Cumulative ^{39}Ar released vs. apparent age diagram for two samples of biotite phenocryst; (B) ^{36}Ar/^{40}Ar versus ^{39}Ar/^{40}Ar isochron plots and age probability from the ^{40}Ar/^{39}Ar step heating experiment for biotite; (C) Incremental heating analyses of one sample of high-Na sanidine; (D) ^{36}Ar/^{40}Ar versus ^{39}Ar/^{40}Ar isochron plots and age probability (plateau only) diagrams. See text for discussion.

southern areas. These events were followed by the emplacement of both the ultramafic (picrite) and the felsic (trachyte) contemporaneous dykes ~ 2 Ma latter, by 86 Ma (86.1 ± 0.5 Ma biotite and 85.9 ± 0.5 Ma K-feldspar ages). The syenites from the São Sebastião and Serraria massifs were potentially emplaced slightly later, as indicated by the high-precision zircon U/Pb ages of 84.8 ± 0.7 Ma and 85 ± 0.3 Ma, respectively (Sato 2006, Sato *et al.* 2008). Comparing high-precision U/Pb and ^{40}Ar/^{39}Ar ages is challenging (e.g., Bachmann *et al.* 2007) but in general the observed differences are within the quoted methods errors in the cases of extrusive rocks or rocks emplaced at high crustal levels, with the ^{40}Ar/^{39}Ar ages being slightly younger. Therefore, the available geochronological data indicate a time span of about 2-4 Ma between the mafic-ultramafic and SiO_2-oversaturated felsic plutonic intrusions and 0-2 Ma between the syenites and the bimodal, mafic-ultramafic and felsic, dykes. Importantly, the geochronological results reveal that dyke emplacement is contemporaneous and likely structurally associated with the intrusion of the São Sebastião Massif.

Our ^{40}Ar/^{39}Ar results, combined with the available U/Pb data, constrain the main alkaline magmatism in the São Sebastião Island within a relatively short time interval, between 87.9 ± 0.7 and 84.8 ± 0.7 Ma. These data, coupled with the crystallization pressure estimate, allow us to obtain a minimum and maximum average post intrusion erosion rate of about 20 and 60 m/Ma, respectively.

Comparisons with nearby and regional alkaline occurrences, and implications

Our results show that the mafic-ultramafic rocks from the layered alkaline occurrences cropping out in the São Sebastião island are coeval with those previously dated at the Monte do Trigo island (Enrich *et al.* 2009)Enrich et al., 2009). Importantly, all the known layered occurrences in these islands are relatively small and certainly represent disrupted fragments of somewhat larger intrusions. As layered intrusions may constitute relatively large igneous complexes, the possibility exists that the occurrences in the São Sebastião Island represent fragments of a major intrusion, later disrupted during the emplacement of the younger syenitic massifs.

The ^{40}Ar/^{39}Ar ages for ultramafic dykes on these islands suggest two distinct magmatic periods, one roughly coeval with the plutonic mafic-ultramafic intrusive complexes (lamprophyre at Monte do Trigo) and other somewhat younger (by 86 ± 0.5 Ma, porphyritic picrite at São Sebastião). Previous K/Ar results suggested an interval between 99 and 88 Ma for the emplacement of mafic-ultramafic, lamprophyric and related rocks (Sonoki and Garda 1988). The available higher

resolution $^{40}Ar/^{39}Ar$ ages suggest, however, a shorter time span from 87.9 ± 0.7 and 84.8 ± 0.7 Ma.

A late peralkaline phonolite dyke in the Monte do Trigo Island has a $^{40}Ar/^{39}Ar$ age around 84.9 ± 1.0 Ma, which is identical to the ages obtained for the SiO_2-oversaturated syenites in the São Sebastião Island, while a porphyritic saturated trachyte intruding the layered sequence in São Sebastião was dated at 86.2 ± 0.65 Ma. Similar felsic dykes are found cutting the São Sebastião Massive, indicating a somewhat younger dyke emplacement event during the magmatic evolution history.

K/Ar and Rb/Sr ages for alkaline silicic rocks from the nearby islands (Vitoria and Búzios, in between *ca*. 84.4 ± 3.9 and 81.4 ± 2.6 Ma, and 101.4 ± 2.1 and 78.0 ± 2.2 (*cf*. Motoki 1986, Alves and Gomes 2001, Gomes *et al*. 2017) are show a relatively broad age rage and large errors (up to ± 4 Ma). Difficulties intrinsic to the K/Ar method and Rb/sr (mineral and whole rock), as well as new insights provided by high resolution geochronology of the São Sebastião Island magmatic rocks, suggest that the regional emplacement of felsic plutonic rocks may have been coeval and new high-precision ages are needed to test this hypothesis.

Towards the continental interior, the average K/Ar ages (87.6 Ma, *cf*. Azzone *et al*. 2009) for the emplacement of the alkaline mafic-ultramafic Ponte Nova Massif overlaps with our results for the coastal islands. The average K/Ar and Rb/Sr age estimates for the main felsic SiO_2-undersaturated syenites in the Poços de Cadas Massif, the largest alkaline occurrence in southern Brazil, are ca. 80-78 Ma (*cf*. Ulbrich *et al*. 1991, Ulbrich *et al*. 2002, Ulbrich *et al*. 2005 and references therein). However, recent high-precision dating results obtained for ultramafic rocks and related breccia as well as hydrothermal rocks are significantly older. In fact, $^{40}Ar/^{39}Ar$ ages in phlogopite crystals from a silico-carbonatitic dyke rock, coeval with phonolite, and from a magmatic breccia containing nepheline syenite fragments, gave 84.8 ± 0.7, (corrected for the Fish Canyon sanidine age of Kuiper *et al*. 2008) and 87.1 ± 0.5 Ma, respectively (Vlach *et al*. 2003, Vlach *et al*. 2018). Also, U/Pb analysis by LA-Quadrupole-ICPMS in zircon from late hydrothermal veins from the massif gave 85.0 ± 2.8 Ma (Takenaka *et al*. 2015). These values are all close and within errors to those obtained for the main alkaline occurrences in the coastal islands and the Ponte Nova Massif, indicating that a significant part of the alkaline magmatism in these areas was roughly coeval.

In São Sebastião and other related alkaline occurrences, chemical and isotopic evidence suggests that the spatial and temporal association of felsic and mafic-ultramafic magmatism results from a complex evolution of magmatic plumbing systems, possibly evolving at different depths and involving partial melting of distinct enriched sources in a heterogeneous mantle, as well as some contributions from crustal sources (cf. Giraldo-Arroyave *et al*. 2018, Giraldo-Arroyave 2020). Although there is little consensus about the genesis of the Late Cretaceous to Paleogene alkaline magmatism in the Serra do Mar Province, our new results and interpretation agree with models arguing that this alkaline magmatism resulted from partial melting of heterogeneous subcontinental mantle sources by a relatively fast decompression event during early stages of continental drift (e.g., Almeida 1983, Comin-Chiaramonti *et al*. 1999, Marques *et al*. 1999, Ernesto *et al*. 2002, Guarino *et al*. 2013), as opposed to plume-related magmatism as proposed by Gibson *et al*. (1995, 1997), Thompson *et al*. (1998) and Sgarbi *et al*. (2004).

CONCLUDING REMARKS

New $^{40}Ar/^{39}Ar$ results and previously available U/Pb-in-zircon high-precision (Sato 2006, Sato *et al*. 2008) ages, supported by geological evidence, better define the main magmatic events recorded in the São Sebastião Island, São Paulo. The first magmatic event corresponds to the emplacement of alkaline mafic-ultramafic layered intrusions by 87.9 ± 0.7 Ma, which was followed by crustal extension and emplacement of a bimodal dyke suite at 86.0 ± 0.8 and 86.1 ± 0.5 Ma, represented by an alkaline mafic-ultramafic porphyritic picrite and a SiO_2-saturated porphyritic trachyte. U/Pd data indicate that the main SiO_2-oversaturated syenitic massifs were emplaced by 84.9 ± 0.5 Ma (average age). We suggest that extension associated with dyke emplacement was genetically linked to the processes controlling the intrusion of the large syenitic massifs in the island.

The geochronological results overlap with the previously determined time interval of alkaline magmatism in the northern segment of the Serra do Mar Alkaline Province (*ca*. 90-80 Ma, *cf*. Gomes *et al*. 2018). In contrast, the geochronological results indicate that the time span of the magmatic events at São Sebastião, which lasted for 4-5 Ma at most, was shorter than previously suggested. It, indicates that a significant part of the alkaline magmatism in the northern sector of the province may have taken place in the same time interval (between 87.9 ± 0.7 and 84.8 ± 0.7 Ma). Importantly, this age interval overlaps with high-precision results recently obtained for the Poços de Caldas Alkaline Massif (by 88-82 Ma, cf. Vlach *et al*. 2003, Takenaka *et al*. 2015, Vlach *et al*. 2018), at the northwest extreme of the Cabo Frio Magmatic Lineament, implying that alkaline magmatism may have been contemporaneous and short-lived along the entire region. A short time span favors a magmatic model where continental rifting along pre-existing crustal weakness zones drove relatively fast decompression-driven partial melting of a heterogeneous enriched mantle and emplacement of a variety of alkaline melts along previous faults (e.g., Comin-Chiaramonti *et al*. 1999). Available crystallization pressure estimates (Giraldo-Arroyave 2020) for the alkaline intrusions also indicate regional post-intrusions exhumation (erosion) rates ranging from 20 to 60 m/Ma.

ACKNOWLEDGMENTS

We thank the staff of the GeoAnalitica at USP, the Cadmium-lined-B-1 CLICIT Facility at Oregon State Univeristy, and the UQ-AGES Laboratory at the University of Queensland. This work was financed by FAPESP (Thematic Projects 2012/06082-6, Coord. E. Ruberti, and 201922084-8, Coord. V. Janasi). M.I. Giraldo-Arroyave benefits from a CNPq doctoral scholarship (Proc. 141781/2015-7). We also thank the two anonymous reviewers for their comments which helped improving the quality of the manuscript.

ARTICLE INFORMATION
Manuscript ID: 20210046. Received on: 06/19/2021. Approved on: 10/08/2021.
MG-A collected and prepared samples, obtained and treated the mineralogical analysis, prepared Figures and Tables and wrote the first manuscript version; SV planed the research, provided general advisorship and improved the manuscript; PV was responsible for $^{40}Ar/^{39}Ar$ data analysis and treatment, provided geochronological advisorship and revised the manuscript.
Competing interests: the authors declare no competing interests.

REFERENCES

Alapieti T.T., Filén B.A., Lahtinen J.J., Lavrov M.M., Smolkin V.F., Voitsekhovsky S.N. 1990. Early Proterozoic layered intrusions in the northeastern part of the Fennoscandian Shield. *Mineralogy and Petrology*, **42**:1-22. https://doi.org/10.1007/BF01162681

Almeida F.F.M. de. 1983. Relações tectônicas das rochas alcalinas Mesozóicas da região meridional da Plataforma Sul-Americana. *Revista Brasileira de Geociências*, **13**(3):139-158. https://doi.org/10.25249/0375-7536.1983133139158

Almeida F.F.M. de, Carneiro R. 1998. Origem e evolucão da Serra do Mar. *Revista Brasileira de Geociências*, **28**(2):135-150.

Alves F.R. 1997. *Contribuição ao conhecimento geológico e petrológico das rochas alcalinas da Ilha dos Búzios, SP*. Tese de Doutoramento. São Paulo: USP. https://doi.org/10.11606/T.44.1997.tde-18092015-174733

Alves F.R., Gomes C.B. 2001. Ilha dos Búzios, litoral norte do Estado de São Paulo: aspectos geológicos e petrográficos. *Geologia USP. Série Científica*, **1**:101-114. https://doi.org/10.5327/S1519-874X2001000100007

Amaral G., Bushee J., Cordani U.G., Kawashita K., Reynolds J.H. 1967. Potassium-argon ages of alkaline rocks from southern Brazil. *Geochimica et Cosmochimica Acta*, **31**(2):117-142. https://doi.org/10.1016/S0016-7037(67)80041-3

Amelin Y.V., Heaman L.M., Semenov V.S. 1995. U/Pb geochronology of layered mafic intrusions in the eastern Baltic Shield: implications for the timing and duration of Paleoproterozoic continental rifting. *Precambrian Research*, **75**(1-2):31-46. https://doi.org/10.1016/0301-9268(95)00015-W

Augusto T. 2003. *Petrografia e quimismo mineral de rochas gábricas e sieníticas do Maciço São Sebastião, Ilha de São Sebastião, SP*. Monografia de Trabalho de Formatura. São Paulo: Instituto de Geociências da Universidade de São Paulo, 50 p.

Azzone R.G., Ruberti E., Rojas G.E.E., Gomes C.B. 2009. Geologia e geocronologia do Maciço Alcalino Máfico-Ultramáfico Ponte Nova (SP-MG). *Revista do Instituto de Geociências*, **9**(2):23-46. https://doi.org/10.5327/Z1519-874X2009000200002

Bachmann O., Oberli F., Dungan M.A., Meier M., Mundil R., Fischer H. 2007. 40Ar/39Ar and U–Pb dating of the Fish Canyon magmatic system , San Juan Volcanic field, Colorado: Evidence for an extended crystallization history. *Chemical Geology*, **236**(1-2):134-166. https://doi.org/10.1016/j.chemgeo.2006.09.005

Bellieni G., Montes-Lauar C.R., De Min A., Piccirillo E.M., Cavazzini G., Melfi A.J., Pacca I.G. 1990. Early and late Cretaceous mgmatism from São Sebastiao Island.pdf. *Geochimica Brasiliensis*, **4**(1):59-83.

Bernstein S., Kelemen P.B., Brooks C.K. 1996. Evolution of the Kap Edvard Holm complex: A mafic intrusion at a rifted continental margin. *Journal of Petrology*, **37**(3):497-519. https://doi.org/10.1093/petrology/37.3.497

Brotzu P., Melluso L., D'Amelio F., Lustrino M. 2005. Potassic dykes and intrusions of the Serra do Mar Igneous Province (SE Brazil). *In*: Comin-Chiaramonti P., Gomes C.B. (eds.), *Mesozoic to Cenozoic alkaline magmatism in the Brazilian Platform*. São Paulo: Edusp/FAPESP, p. 443-472.

Comin-Chiaramonti P., Cundari A., DeGraff J., Gomes C.B., Piccirillo E.M. 1999. Early Cretaceous-Terciary magmatism in Eastern Paraguay (western Paraná basin): geological, geophysical and geochemical relationships. *Journal of Geodynamics*, **28**(4):375-391. https://doi.org/10.1016/S0264-3707(99)00016-2

Comin-Chiaramonti P., Cundari A., Piccirillo E.M., Gomes C.B., Castorina F., Censi P., De Min A., Marzoli A., Speziale S., Velázquez V.F. 1997. Potassic and sodic igneous rocks from Eastern Paraguay: Their origin from the lithospheric mantle and genetic relationships with the associated Paraná flood tholeiites. *Journal of Petrology*, **38**(4):495-528. https://doi.org/10.1093/petroj/38.4.495

Coutinho J.M.V., Melcher G.C. 1973. Levantamento geológico e petrográfico na Ilha do Monte de Trigo (Litoral norte de São Paulo, Brasil). *Revista Brasileira de Geociencias*, **3**(4):243-256.

Deckart K., Féraud G., Marques L.S., Bertrand H. 1998. New time constraints on dyke swarms related to the Paraná-Etendeka magmatic province, and subsequent South Atlantic opening, southeastern Brazil. *Journal of Volcanology and Geothermal Research*, **80**(1-2):67-83. https://doi.org/10.1016/S0377-0273(97)00038-3

Deino A., Potts R. 1990. Single-crystal 40Ar/39Ar dating of the Olorgesailie Formation, southern Kenya Rift. *Journal of Geophysical Research: Solid Earth*, **95**(B6):8453-8470. https://doi.org/10.1029/JB095iB06p08453

Eales H.V, Cawthorn R.G. 1996. The Bushveld Complex. *Developments in Petrology*, **15**:181-229. https://doi.org/10.1016/S0167-2894(96)80008-X

Emeleus C.H., Cheadle M.J., Hunter R.H., Upton B.G.J., Wadsworth W.J. 1996. The Rum Layered Suite. *Developments in Petrology*, **15**:403-439. https://doi.org/10.1016/S0167-2894(96)80014-5

Enrich G.E.R. 2005. Petrogênese da suíte alcalina da Ilha Monte de Trigo, SP. Tese de Doutoramento. São Paulo: Universidade de São Paulo, 229 p. https://doi.org/10.11606/T.44.2006.tde-04022014-164218

Enrich G.E.R., Azzone R.G., Ruberti E., Gomes C.B., Comin-chiaramonti P. 2005. Itatiaia, Passa Quatro and São Sebastião island, the major alkaline syenitic complex from the Serra do Mar region. *In*: Comin-Chiaramonti P., Gomes C.B. (eds.), *Mesozoic to Cenozoic alkaline magmatism in the Brazilian Platform*. São Paulo: Edusp/FAPESP, p. 419-442.

Enrich G.E.R., Ruberti E., Gomes C. de B. 2009. Geology and geochronology of Monte de Trigo island alkaline suite, southeastern Brazil. *Revista Brasileira de Geociências*, **39**(1):67-80. https://doi.org/10.25249/0375-7536.20093916780

Ernesto M., Marques L.S., Piccirillo E.M., Molina E.C., Ussami N., Comin-Chiaramonti P., Bellieni G. 2002. Paraná Magmatic Province-Tristan da Cunha plume system: Fixed versus mobile plume, petrogenetic considerations and alternative heat sources. *Journal of Volcanology and Geothermal Research*, **118**(1-2):15-36. https://doi.org/10.1016/S0377-0273(02)00248-2

Ernst R.E., Buchan K.L., Campbell I.H. 2005. Frontiers in Large Igneous Province research. *Lithos*, **79**(3-4):271-297. https://doi.org/10.1016/j.lithos.2004.09.004

Fleck R.J., Sutter J.F., Elliot D.H. 1977. Interpretation of discordant 40Ar/39Ar age-spectra of mesozoic tholeiites from antarctica. *Geochimica et Cosmochimica Acta*, **41**(1):15-32. https://doi.org/10.1016/0016-7037(77)90184-3

Freitas R. 1947. Geologia e petrologia da Ilha de São Sebastião. *Boletim da Faculdade de Filosofia, Ciências e Letras da Universidade de São Paulo*, **85**:1-244.

Gibson S.A., Thompson R.N., Leonardos O.H., Dickin A.P., Mitchell J.G. 1995. The late cretaceous impact of the trindade mantle plume: Evidence from large-volume, mafic, potassic magmatism in SE Brazil. *Journal of Petrology*, **36**(1):189-229. https://doi.org/10.1093/petrology/36.1.189

Gibson S.A., Thompson R.N., Weska R.K., Dickin A.P., Leonardos O.H. 1997. Late Cretaceous rift-related upwelling and melting of the Trindade starting mantle plume head beneath western Brazil. *Contributions to Mineralogy and Petrology*, **126**:303-314. https://doi.org/10.1007/s004100050252

Giraldo-Arroyave M.I. 2020. *Geology and petrology of the Frade Alkaline Mafic-Ultramafic Layered Complex in the São Sebastião Island, Southeastern Brazil*. Tese de Doutoramento. São Paulo: Universidade de São Paulo, 289 p. https://doi.org/10.11606/T.44.2020.tde-26012021-163726

Giraldo-Arroyave M.I., Vlach S.R.F., Simonetti A. 2018. Trace element and Hf isotope composition in primary zircons from the São Sebastião Pluton, SP, Brazil and implications. *In*: South American Symposium on isotope Geology. *Proceedings…*

Gomes A.S., Vasconcelos P.M. 2021. Geochronology of the Paraná-Etendeka large igneous province. *Earth-Science Reviews*, **220**:103716. https://doi.org/10.1016/j.earscirev.2021.103716

Gomes C.B., Alves F.R., Azzone R.G., Rojas G.E.E., Ruberti E. 2017. Geochemistry and petrology of the Búzios Island alkaline massif, SE, Brazil. *Brazilian Journal of Geology*, **47**(1):127-145. https://doi.org/10.1590/2317-4889201720160121

Gomes C.B., Azzone R.G., Ruberti E., Vasconcelos P.M., Sato K., Enrich G.E.R. 2018. New age determinations for the Banhadão and Itapirapuã complexes in the Ribeira Valley, southern Brazil. *Brazilian Journal of Geology*, **48**(2):403-414. https://doi.org/10.1590/2317-4889201820170094

Gualda G.A.R., Vlach S.R.F. 2005. Stoichiometry-based estimates of ferric iron in calcic, sodic-calcic and sodic amphiboles: A comparison of various methods. *Anais da Academia Brasileira de Ciências*, **77**(3):521-534. https://doi.org/10.1590/S0001-37652005000300012

Gualda G.A.R., Vlach S.R.F. 2007. The Serra da Graciosa A-type Granites and Syenites, southern Brazil. Part 2: Petrographic and mineralogical evolution of the alkaline and aluminous associations. *Lithos*, **93**(3-4):310-327. https://doi.org/10.1016/j.lithos.2006.06.002

Guarino V., Wu F., Lustrino M., Melluso L., Brotzu P., Gomes C.B., Ruberti E., Tassinari C.C.G., Svisero D.P. 2013. U – Pb ages , Sr – Nd- isotope geochemistry, and petrogenesis of kimberlites, kamafugites and phlogopite-picrites of the Alto Paranaíba Igneous Province, Brazil. *Chemical Geology*, **353**:65-82. https://doi.org/10.1016/j.chemgeo.2012.06.016

Harrison T.M., McDougall I. 1981. Excess 40Ar in metamorphic rocks from Broken Hill, New South Wales: implications for 40Ar/39Ar age spectra and the thermal history of the region. *Earth and Planetary Science Letters*, **55**(1):123-149. https://doi.org/10.1016/0012-821X(81)90092-3

Hawthorne F.C., Oberti R., Harlow G.E., Maresch W.V, Martin R.F., Schumacher J.C., Welch M.D. 2012. Nomenclature of the amphibole supergroup. *American Mineralogist*, **97**(11-12):2031-2048. https://doi.org/10.2138/am.2012.4276

Heilbron M., Machado N. 2003. Timing of terrane accretion in the Neoproterozoic-Eopaleozoic Ribeira Orogen (se Brazil). *Precambrian Research*, **125**(1-2):87-112. https://doi.org/10.1016/S0301-9268(03)00082-2

Hennies W.T., Hasui Y. 1977. Contribuição ao conhecimento da geologia da Ilha de São Sebastião. *In*: Simpósio Regional de Geologia, 1., São Paulo. *Proceedings...*, p. 199-209.

Hora J.M., Singer B.S., Jicha B.R., Beard B.L., Johnson C.M., Silva S. de, Salisbury M. 2010. Volcanic biotite-sanidine 40Ar/39Ar age discordances reflect Ar partitioning and pre-eruption closure in biotite. *Geology*, **38**(10):923-926. https://doi.org/10.1130/G31064.1

Jourdan F., Renne P.R. 2007. Age calibration of the Fish Canyon sanidine 40Ar/39Ar dating standard using primary K-Ar standards. *Geochimica et Cosmochimica Acta*, **71**(2):387-402. https://doi.org/10.1016/j.gca.2006.09.002

Kuiper K.F., Deino A., Hilgen F.J., Krijgsman W., Renne P.R., Wijbrans J.R. 2008. Synchronizing Rock Clocks of Earth History. Science, **320**(5875):500-504. https://doi.org/10.1126/science.1154339

Leake B.E., Woolley A.R., Arps C.E.S., Birch W.D., Gilbert M.C., Grice J.D., Hawthorne Ec., Kato A., Kisch H.J., Krivovichev V.G., Linthout K., Laird J., Mandarino J., Maresch W.V., Nickel E.H., Rock N.M.S., Schumacher J.C., Smith D.C., Stephenson N.C.N., Ungaretti L., Whittaker E.J.W., Youzhi G. 1997. Nomenclature of amphiboles. Report of the Subcommittee on Amphiboles of the International Mineralogical Association, Commission on New Minerals and Mineral Names. *American Mineralogist*, 9(3):623-651. https://doi.org/10.1127/ejm/9/3/0623

Lee J.Y., Marti K., Severinghaus J.P., Kawamura K., Yoo H.S., Lee J.B., Kim J.S. 2006. A redetermination of the isotopic abundances of atmospheric Ar. *Geochimica et Cosmochimica Acta*, **70**(17):4507-4512. https://doi.org/10.1016/j.gca.2006.06.1563

Lima G.A. 2001. *Gabros estratiformes da região norte da Ilha de São Sebastião, SP*. Dissertação de Mestrado. São Paulo: Instituto de Geociências da Universidade de São Paulo, 170 p. https://doi.org/10.11606/D.44.2001.tde-25092015-160340

Marques L.S., Dupré B., Piccirillo E.M. 1999. Mantle source compositions of the Parana Magmatic Province (southern Brazil): Evidence from trace element and Sr-Nd-Pb isotope geochemistry. *Journal of Geodynamics*, **28**(4-5):439-458. https://doi.org/10.1016/S0264-3707(99)00020-4

McCallum I.S. 1996. The Stillwater Complex. *Developments in Petrology*, **15**:441-483. https://doi.org/10.1016/S0167-2894(96)80015-7

McDougall I., Wellman P. 2011. Calibration of GA1550 biotite standard for K/Ar and 40Ar/39Ar dating. *Chemical Geology*, **280**(1-2):19-25. https://doi.org/10.1016/j.chemgeo.2010.10.001

Montes-Lauar C.R., Pacca I.G., Melfi A.J., Kawashita K. 1995. Late Cretaceous alkaline complexes, southeastern Brazil: Paleomagnetism and geochronology. *Earth and Planetary Science Letters*, **134**(3-4):425-440. https://doi.org/10.1016/0012-821X(95)00135-Y

Morimoto N., Fabries J., Ferguson A.K., Ginzburg I.V., Ross M., Seifert F.A., Zussman J., Aoki K., Gottardi G. 1988. Nomenclature of pyroxenes Subcommittee. *American Mineralogist*, **73**(9-10):1123-1133.

Motoki A. 1986. *Geologia e petrologia do maciço alcalino da Ilha de Vitória, SP*. Tese de Doutoramento. São Paulo: Instituto de Geociências, Universidade de São Paulo, 245 p. https://doi.org/10.11606/T.44.1986.tde-30062015-101540

Pabst L. 2014. *Gabros estratiformes e sienitos supersaturados da Ilha de São Sebastião, SP: relações geológicas e petrografia na região da Ponta da Sepituba*. Monografia de Trabalho de Formatura. São Paulo: Universidade de São Paulo, 46 p.

Piccirillo E.M., Bellieni G., Cavazzini G., Comin-Chiaramonti P., Petrini R., Melfi A.J., Pinese J.P.P., Zantadeschi P., De Min A. 1990. Lower Cretaceous tholeiitic dyke swarms from the Ponta Grossa Arch (southeast Brazil): Petrology, Sr-Nd isotopes and genetic relationships with the Paraná flood volcanics. *Chemical Geology*, **89**(1-2):19-48. https://doi.org/10.1016/0009-2541(90)90058-F

Renne P.R., Deckart K., Ernesto M., Féraud G., Piccirillo E.M. 1996. Age of the Ponta Grossa dyke swarm (Brazil), and implications to Paraná flood volcanism. *Earth and Planetary Science Letters*, **144**(1-2):199-211. https://doi.org/10.1016/0012-821x(96)00155-0

Renne P.R., Ernesto M., Pacca I.G., Coe R.S., Glen J.M., Prévot M., Perrin M. 1992. The age of Paraná flood volcanism, rifting of Gondwanaland, and the Jurassic-Cretaceous boundary. Science, **258**(5084):975-979. https://doi.org/10.1126/science.258.5084.975

Riccomini C., Velázquez V.F., Gomes C.B. 2001. Cenozoic lithospheric faulting in the Asunción Rift, eastern Paraguay. *Journal of South American Earth Sciences*, **14**(6):625-630. https://doi.org/10.1016/S0895-9811(01)00037-2

Riccomini C., Velázquez V.F., Gomes C.B. 2005. Mesozoic to Cenozoic alkaline magmatism in central-southeastern Brazilian Platform. *In*: Comin-Chiaramonti P., Gomes, C.B. (eds.), *Mesozoic to Cenozoic alkaline magmatism in the Brazilian Platform*. São Paulo: Edusp/FAPESP, v. 123, p. 31-55.

Rieder M., Cavazzini G., D'yakonov Y.S., Frank-Kamenetskii V.A., Gottardi G., Guggenheim S., Koval P.V., Müller G., Neiva A.M.R., Radoslovich E.W., Robert J.-L., Sassi F.P., Takeda H., Weiss Z., Wones D.R. 1998. Nomenclature of the Micas. *The Canadian Mineralogist*, **46**:586-595. https://doi.org/10.1346/CCMN.1998.0460513

Sato E. 2006. *Petrografia e geocronologia U/Pb (TIMS) de rochas alcalinas da Ilha de São Sebastião (SP)*. Monografia de Trabalho de Formatura. São Paulo: Universidade de São Paulo, 56 p.

Sato E., Vlach S.R., Basei M.A.S. 2008. Zircon and baddeleyite U-Pb dating (TIMS) of mesozoic alkaline rocks from the São Sebastião Island, southeastern Brazil. *In*: International Geological Congress, Oslo. *Proceedings…*

Sgarbi B.A., Heaman L.M., Gaspar C. 2004. U – Pb perovskite ages for brazilian kamafugitic rocks : further support for a temporal link to a mantle plume hotspot track. Journal of South American Earth Sciences, **16**(8):715-724. https://doi.org/10.1016/j.jsames.2003.12.005

Sonoki I.K., Garda G.M. 1988. Idades K-Ar de rochas alcalinas do Brasil Meridional e Paraguai Oriental: compilação e adaptação às novas constantes de decaimento. *Boletim IG-USP. Série Científica*, **19**:63-85. https://doi.org/10.11606/issn.2316-8986.v19i0p63-85

Steiger R.H., Jäger E. 1977. Subcomission on geochronology: Convection on the use of decay constants in geo- and cosmochronology. *Earth and Planetary Science Letters*, **36**(3):359-362. https://doi.org/10.1016/0012-821X(77)90060-7

Takenaka L.B., Lana C., Scholz R., Nalini Jr. H.A., Abreu A.T. 2015. Optimization of the in-situ U-Pb age dating method via LA-Quadrupole-ICP-MS with applications to the timing of U-Zr-Mo mineralization in the Poços de Caldas Alkaline Complex, SE Brazil. *Journal of South American Earth Sciences*, **62**:70-79. https://doi.org/10.1016/j.jsames.2015.04.007

Thiede D.S., Vasconcelos P.M. 2010. Paraná flood basalts: Rapid extrusion hypothesis confirmed by new 40Ar/39Ar results. *Geology*, 38(8):747-750. https://doi.org/10.1130/G30919.1

Thompson R.N., Gibson S.A., Mitchell J.G., Dickin A.P., Leonardos O.H., Brod J.A., Greenwood J.C. 1998. Migrating Cretaceous–Eocene Magmatism in the Serra do Mar Alkaline Province, SE Brazil: Melts from the Deflected Trindade Mantle Plume? *Journal of Petrology*, **39**(8):1493-1526. https://doi.org/10.1093/petroj/39.8.1493

Timich M., Eduardo G., Rojas E., Ruberti E., Gomes C.D.B. 2019. Relações de contato entre rochas alcalinas máficas e sieníticas na Praia do Jabaquara, setor norte da Ilha de São Sebastião, SP. *Geologia USP. Série Científica*, **19**(4):3-22. https://doi.org/10.11606/issn.2316-9095.v19-157121

Turner S., Regelous M., Kelley S., Hawkesworth C., Mantovani M. 1994. Magmatism and continental break-up in the South Atlantic: high precision 40Ar/39Ar geochronology. *Earth and Planetary Science Letters*, **121**(3-4):333-348. https://doi.org/10.1016/0012-821X(94)90076-0

Ulbrich H.H.G.J., Garda G.M., Ulbrich M.N.C. 1991. Avaliação das idades K/Ar dos maciços alcalinos do Brasil Sul-oriental e Paraguai oriental. Boletim de Geociências-Petrobras, (9):87-92. https://doi.org/10.11606/issn.2317-8078.v0i9p87-92

Ulbrich H.H.G.J., Gomes C.B. 1981. Alkaline rocks from continental Brazil. *Earth Science Reviews*, **17**(1-2):135-154. https://doi.org/10.1016/0012-8252(81)90009-X

Ulbrich H.H.G.J., Vlach S.R.F., Demaiffe D., Ulbrich M.N.C. 2005. Structure and origin of the Poços de Caldas alkaline massif, SE Brazil. *In*: Comin-Chiaramonti P., Gomes C.B. (eds.), *Mesozoic to Cenozoic alkaline magmatism in the Brazilian Platform*. São Paulo: Edusp/FAPESP, p. 367-418.

Ulbrich H.H.G.J., Vlach S.R.F., Ulbrich M.N.C., Kawashita K. 2002. Penecontemporaneous syenitic-phonolitic and basic-ultrabasic-carbonatitic rocks at the Poços de Caldas alkaline massif, SE Brazil: geologic and geochronologic evidence: *Revista Brasileira de Geociências*, **32**(1):15-26.

Vasconcelos P.M., Onoe A.T., Kawashita K., Soares A.J., Teixeira W. 2002. 40Ar/39Ar geochronology at the Instituto de Geociências, USP: Instrumentation, analytical procedures, and calibration. *Anais da Academia Brasileira de Ciencias*, **74**(2):297-342. https://doi.org/10.1590/S0001-37652002000200008

Velázquez V. 1996. *Provincia Alcalina Alto Paraguay: caracteristicas petrograficas geoquimicas y geocronologicas*. Tese de Doutoramento. São Paulo: Universidade de São Paulo, 101 p. https://doi.org/10.11606/T.44.1996.tde-22122015-142543

Villa I.M. 1998. Isotopic closure. *Terra Nova*, **10**(1):42-47. https://doi.org/10.1046/j.1365-3121.1998.00156.x

Vlach S.R.F., Ulbrich H.H.G.J., Ulbrich M.N.C., Vasconcelos P.M. 2018. Melanite-bearing nepheline syenite fragments and 40Ar/39Ar age of phlogopite megacrysts in conduit breccia from the Poços de Caldas Alkaline Massif (MG/SP), and implications. *Brazilian Journal of Geology*, 4 https://doi.org/10.1590/2317-48892018201700958(2):391-402. https://doi.org/10.1590/2317-4889201820170095

Vlach S.R.F., Vilalva F.C.J., Ulbrich M.N.C., Ulbrich H.H.G.J., Vasconcelos P.M. 2003. Phlogopite from carbonatitic veins associated with the Poços de Caldas Alkaline Massif, SE Brazil: mineralogy and 40Ar/39Ar dating by the laser step heating method. *In*: South American Symposium on Isotope Geology, 4., Salvador. *Proceedings…*, p. 702-705.

White R., McKenzie D. 1989. Magmatism at rift zones: the generation of volcanic continental margins and flood basalts. *Journal of Geophysical Research*, **94**(B6):7685-7729. https://doi.org/10.1029/JB094iB06p07685

Wilson J.R., Robins B., Nielsen F.M., Duchesne J.C., Vander Auwera J. 1996. The Bjerkreim-Sokndal Layered Intrusion, Southwest Norway. *Developments in Petrology*, **15**:231-255. https://doi.org/10.1016/S0167-2894(96)80009-1